catalysts

MDPI

Review

Bismuth-Based Multi-Component Heterostructured Nanocatalysts for Hydrogen Generation

Saman Shaheen, Iqra Sadiq, Syed Asim Ali and Tokeer Ahmad *

Nanochemistry Laboratory, Department of Chemistry, Jamia Millia Islamia, New Delhi 110025, India
* Correspondence: tahmad3@jmi.ac.in; Tel.: +91-11-26981717 (ext. 3261)

Abstract: Developing a unique catalytic system with enhanced activity is the topmost priority in the science of H_2 energy to reduce costs in large-scale applications, such as automobiles and domestic sectors. Researchers are striving to design an effective catalytic system capable of significantly accelerating H_2 production efficiency through green pathways, such as photochemical, electrochemical, and photoelectrochemical routes. Bi-based nanocatalysts are relatively cost-effective and environmentally benign materials which possess advanced optoelectronic properties. However, these nanocatalysts suffer back recombination reactions during photochemical and photoelectrochemical operations which impede their catalytic efficiency. However, heterojunction formation allows the separation of electron–hole pairs to avoid recombination via interfacial charge transfer. Thus, synergetic effects between the Bi-based heterostructured nanocatalysts largely improves the course of H_2 generation. Here, we propose the systematic review of Bi-based heterostructured nanocatalysts, highlighting an in-depth discussion of various exceptional heterostructures, such as $TiO_2/BiWO_6$, $BiWO_6/Bi_2S_3$, $Bi_2WO_6/BiVO_4$, Bi_2O_3/Bi_2WO_6, $ZnIn_2S_4/BiVO_4$, Bi_2O_3/Bi_2MoO_6, etc. The reviewed heterostructures exhibit excellent H_2 evolution efficiency, ascribed to their higher stability, more exposed active sites, controlled morphology, and remarkable band-gap tunability. We adopted a slightly different approach for reviewing Bi-based heterostructures, compiling them according to their applicability in H_2 energy and discussing challenges, prospects, and guidance to develop better and more efficient nanocatalytic systems.

Keywords: nanocatalysis; heterojunctions; water splitting; hydrogen energy; sustainable energy

check for updates

Citation: Shaheen, S.; Sadiq, I.; Ali, S.A.; Ahmad, T. Bismuth-Based Multi-Component Heterostructured Nanocatalysts for Hydrogen Generation. *Catalysts* **2023**, *13*, 295. https://doi.org/10.3390/catal13020295

Academic Editor: Yuanhua Sang

Received: 21 November 2022
Revised: 12 January 2023
Accepted: 16 January 2023
Published: 28 January 2023

Copyright: © 2023 by the authors. Licensee MDPI, Basel, Switzerland. This article is an open access article distributed under the terms and conditions of the Creative Commons Attribution (CC BY) license (https://creativecommons.org/licenses/by/4.0/).

1. Introduction

As the demographic transition theory indicates, the world's population has increased explosively and simultaneously galvanized many problems, such as the energy crisis, global warming, environmental pollution, and degradation of fossil fuels. In order to combat these problems, researchers envisage green energy resources will support economically sustainable development as an alternative to existing energy resources, propelling this as the ultimate challenge for the research community [1]. According to statistical analysis, it is speculated that by 2050, energy consumption will be nearly 27 terawatts (TW), which is not practically sustainable using fossil derivative fuels. Hence, the development of renewable energy sources (RES) is of critical importance, as some variables, such as population growth and global food supply, cannot be significantly modified [2]. According to the report by the International Energy Agency (IEA) on net-zero policy, there will be slowing in global temperature elevation by 2050 through taking green pathways instead of non-renewable energy sources [3]. Hydrogen (H_2) generation has attracted much attention, as it is the most viable replacement for fossil fuels in the future, owing to its escalated efficiency [4]. Precursors of clean H_2 fuel are available abundantly; however, the challenges associated with their cost of efficient production are multifarious. Innovative socio-economic policies and research developments are urgently needed for the sustainability of an H_2 economy. In order to harness H_2 as an energy source in the long term and to enhance the share of

renewable energy in total energy consumption, several developing and developed nations are investing in the sustainable energy sector. Global accords that are internationally mutually agreed upon can serve as the building blocks of an environmentally viable H_2 pathway [5].

H_2 production from fossil fuels is a major concern, as it extensively depletes fossil fuels, causing chain reactions that influence the global climatic and exogenic phenomena. Furthermore, the ample use of non-renewable energy sources, such as burning fossil fuels, increases anthropogenic carbon dioxide (CO_2) emissions and is responsible for the greenhouse effect and climate change resulting from increasing global temperature. H_2 fuel is non-toxic, abundantly available and inexpensive, and has higher energy than natural gasoline, along with higher gravimetric energy density, i.e., high energy-to-weight ratio [6]. The significant challenge for the H_2 economy is the storage of H_2, as it is flammable due to a low ignition temperature that leads to explosion [7]. It is not stored underground, as it has a high escaping tendency because of its small size. The odorless, colorless, and tasteless properties of H_2 make it difficult to detect by physical methods. Currently, two main problems arise in the energy sector: the rise in global temperature and degradation of fossil fuels. Most of the needs for energy consumption are fulfilled by fossil fuels and natural gas, directly leading to the depletion of non-renewable energy sources and ultimately causing environmental hazards [8–10]. It is essential to raise awareness about renewable energy for sustainable development to minimize the world's energy crisis.

There are many other renewable energy sources, such as wind energy, thermal energy, biomass, etc. [11], and amongst them, solar energy is the most prominent, abundantly available energy, a major reason for the substitution of non-renewable energy sources using solar energy. Solar energy is favorable for H_2 production because, unlike fossil fuels, it is a green and clean energy source with higher efficiency for energy conversion. Visible, light-activated materials account for about 43% of the solar spectrum, while UV light-active semiconductors make up only 5% [12]. This necessitates the importance of developing visible light-active catalytic systems. Fujishima and Honda carried out photoelectrochemical water splitting studies on TiO_2 in 1972 [13]. Since then, H_2 generation using overall water splitting (OWS) has attracted much attention, and has been considered as the most sustainable, renewable, and clean energy source. It is a very efficient approach, as water is the starting material and also the byproduct of the energy conversion process [14,15]. Various routes, such as photocatalytic (PC), electrocatalytic (EC), and photo-electrocatalytic (PEC) pathways, are preferred for OWS applications [16]. Multifunctional nanocatalysts for water splitting are urgently needed for carrying out diverse optoelectronic, multiferroic, and sustainable energy applications, as they possess more exposed sites than the bulk catalysts [17,18].

Among the fundamental approaches to water splitting, semiconductor photocatalysis has an immense potential to split water into H_2 and O_2. There are two reactions that occur: one is the H_2 evolution reaction (HER), in which H^+ accepts an electron to produce H_2; and the O_2 evolution reaction (OER), in which holes participate in the evolution of O_2 by reacting with water. Water splitting is an endothermic process, with a very large free energy value of ΔG ~237 KJ/mol, and is known as an "up-hill" reaction [19]. Oxidation and reduction reactions occur at the respective reaction sites. Few photocatalytic systems are active under UV irradiation. However, for higher efficiency, one needs a catalyst with a narrow band range in the visible light region for enhanced light absorption, leading to effective OWS [20].

According to band theory, the semiconductor contains the conduction band (CB), valence band (VB), and energy levels between VB and CB. The band structure of the semiconductors has discontinuous energy bands [21–23]. The oxidation and reduction of photogenerated holes and electrons depend on the positioning of VB and CB, respectively. After irradiating with light, semiconductor photocatalysts exhibit photoexcitation, due to which electrons jump from the VB to the CB, leaving a hole in the VB and then diffusing the photogenerated charges at the surface of the semiconductor. In the case of water splitting,

H^+ accepts an electron to produce H_2, while in the case of pollutant degradation, electrons are captured by O_2 to produce superoxide radicals. The primary focus of the researchers is the development of nanocatalysts that can excellently carry out OWS operations [22]. Other important routes for green H_2 energy production are electrocatalysis and photoelectrocatalysis. In an electrocatalysis reaction, water splitting is composed of two electrodes, and HER and OER reactions occur at the respective electrode. A more efficient catalytic system in OWS is a promising candidate for replacing fossil fuels with traditional H_2 generation. However, a higher overpotential is needed to overcome the sluggish kinetics in EC applications. In photoelectrocatalysis, the cell comprises of photoanodes and photocathodes [14,20]. Generally, p-type and n-type semiconductors have been exploited for photocathodes and photoanodes, respectively. A high photocurrent density is needed for enhanced PEC efficiency [22,23].

The various Bi-based compounds are exploited in the PC and PEC applications owing to tremendous physicochemical features such as narrow band gap of less than 3 eV, appropriate band alignment, excellent optoelectronic properties, non-toxicity, low cost, and excellent light-driven ability, which preferably occurs in the visible region. Along with their exploitability in HER, OER, and pollutant degradation, Bi-based compounds also have plenty of applications in industrial sector [24]. In the past few years, many Bi-based nanocatalysts have been utilized in OWS applications, such as Bi_2O_3 [25], $BiPO_4$ [26], $BiVO_4$ [27], BiOCl [28], Bi_2Mo_6 [29], etc., but have exhibited nominal catalytic efficiencies because of the swift recombination of photogenerated charge carriers, photo-corrosiveness, and chemical instability due to exceptionally reductive electrons and oxidative holes. Some modifications have been developed to obtain the optimum catalytic efficiency of the Bi-based nanocatalysts. Semiconductor nanocatalysts synthesized by different methods have different sizes, structures, and optoelectronic properties and have their pros and cons [30]. Various methods, such as doping with other metals and nonmetals, building heterostructures, surface atom reconstructions/modifications, morphology control, etc., ensure the accelerated performance of Bi-based nanocatalysts [31]. There is expeditious research on Bi-based heterostructured nanocatalysis conducted year by year, as demonstrated in Figure 1.

Bi-based oxides contain 6s orbital of Bi and 2p orbital of oxygen in the VB making, making them more favorable than other oxides such as TiO_2, a well-known photocatalytic material that has a wide band gap of ~3.2 eV [32]. PEC water splitting with TiO_2 has been studied for a long time, but it is less effective as the band gap lies in the UV region. Metal nitrides, sulfides, and oxides are favorable photoelectrodes, but metal oxides are generally explored due to their low cost and stability. Bi-based composite oxides are cost-effective and contain a perovskite-type structure with the general formula ABX_3, in which the 'A' atom contains rare earth metals, and the 'B' atom has transition metals, and 'X' can be oxides or halides. Perovskite oxide is an excellent multiferroic material with optoelectronic properties. Bi_2WO_6 is an Aurivillius phase material with a band gap of ~2.8 eV and an orthorhombic structure [33]. It combines with other semiconductors to improve the visible range, separation of charge carriers, photo-corrosion, and stability of the catalysts.

Bi_2WO_6 forms heterojunction with $ZnIn_2S_4$ to improve the catalytic efficiency of OWS [34]. $BiVO_4$ shows exceptional photocatalytic activity with a band gap of ~2.4 eV but undergoes a recombination reaction. For an efficient H_2 generation, Z-scheme $ZnIn_2S_4$/$BiVO_4$ heterojunction is effectively employed. The rate of photocatalytic H_2 production is 5944 μmol h^{-1}, five times higher than that of bare $ZnIn_2S_4$ [35]. Bi_2MoO_6 exhibits excellent light-driven properties, showing a band gap of 2.7–2.8 eV. It is chemically stable, cost-effective, and non-toxic. It is a very effective catalyst showing excellent optoelectronic properties and is used for water splitting and for pollutant degradation applications [36]. The Bi_2S_3/Ni_3S_2/NF (Nickel Foam) heterostructure electrocatalyst exhibits a low overpotential of 268 mV at 10 mA cm^{-2} and low Tafel slope of 82 $mVdec^{-1}$, leading to a high electrocatalytic performance with a strong synergistic effect [37]. High current density and low Tafel slope are the ultimate requirements for a better electrocatalyst. The

$BiVO_4/WO_3/SnO_2$ ternary heterostructured photoelectrocatalyst delivers higher photocurrent density as high as 3.1 $mAcm^{-2}$, and maximum incident photon-to-current conversion efficiencies (IPCE) of ~70% with enhanced PEC activity [38]. Therefore, this review endeavors to summarize the various promising Bi-based heterostructured nanocatalysts such as TiO_2/Bi_2WO_6, Bi_2WO_6/Bi_2S_3, $Bi_2WO_6/BiVO_4$, Bi_2O_3/Bi_2WO_6, $ZnIn_2S_4/BiVO_4$, and Bi_2O_3/Bi_2MoO_6, which have made steady progress so far in the development of water splitting for effective H_2 generation.

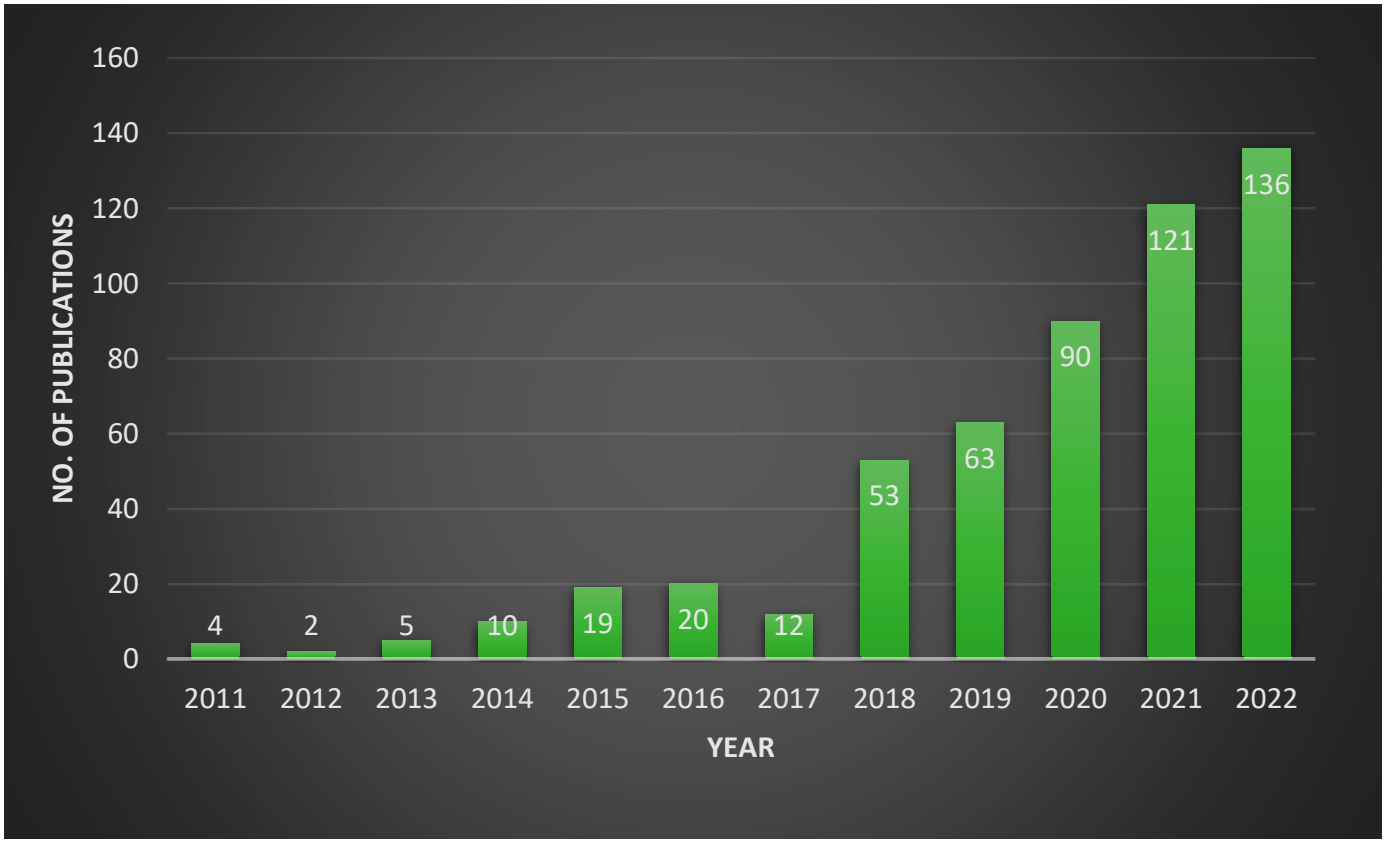


Figure 1. No. of publications "Bismuth based heterostructure" (data obtained from Scopus on 30 September 2022).

2. Scope of the Review

Hitherto, there are many reviews on the various Bi-based nanocatalysts for organic degradation [39], environmental applications [40], fuel production [41], water treatment [42], air purification [43], and CO_2 reduction [44]. There are sporadic reviews which highlight the importance of Bi-based heterostructures towards green energy production [45,46]. Some reviews also have a proclivity for various modification strategies [47]. Due to their advanced physicochemical properties, Bi-based heterostructures attain a lot of interest in PC, EC, and PEC applications. However, we could not find a review that discusses their applicability in the PC, EC, and PEC pathways of H_2 generation under a single umbrella. Therefore, this review merely focuses on Bi-based heterostructured nanocatalysts for varied applications in PC, EC, and PEC for H_2 production.

3. Heterojunctions

Heterostructures are composite materials (conductor, semiconductor, or insulator) that contain an interface between two or more different materials known as heterojunctions. The schematic diagram of heterojunction formation is illustrated in Figure 2. Heterojunction formation tends to separate electron–hole pairs from restraining charge recombination. It helps retain the redox reactions at different sites and maintain energy band gaps [48]. Heterostructures constructed from two other semiconductors improve light absorption ability and enhance charge separation due to the interface effect [36]. Upon irradiation, the photogenerated electrons and holes are enforced between the interface, exhibiting an electric field. The photoexcited electrons and holes can only be transferred from a wide bandgap to a narrow band gap. The very conceptual framework of heterostructure comes from semiconductor physics. It is a very effective method for the modification of catalytic activity towards PC and PEC applications, as the heterostructure formation tremendously subdues the recombination of charge carriers for PC and PEC applications, improves the transport properties, modifies active sites, etc. The various heterojunctions show distinct catalytic applications. The four major types of heterojunctions for charge separations are (a) Type II heterojunctions, (b) Z-scheme heterojunctions, (c) p–n heterojunctions, and (d) Schottky heterojunctions [49,50], as demonstrated in Figure 3. The Z-scheme and p–n heterojunctions have an internal electric field (IEF) at the junctions of two different composite materials, which is productive in carrier charge transfer, relating to separation under excitation conditions.

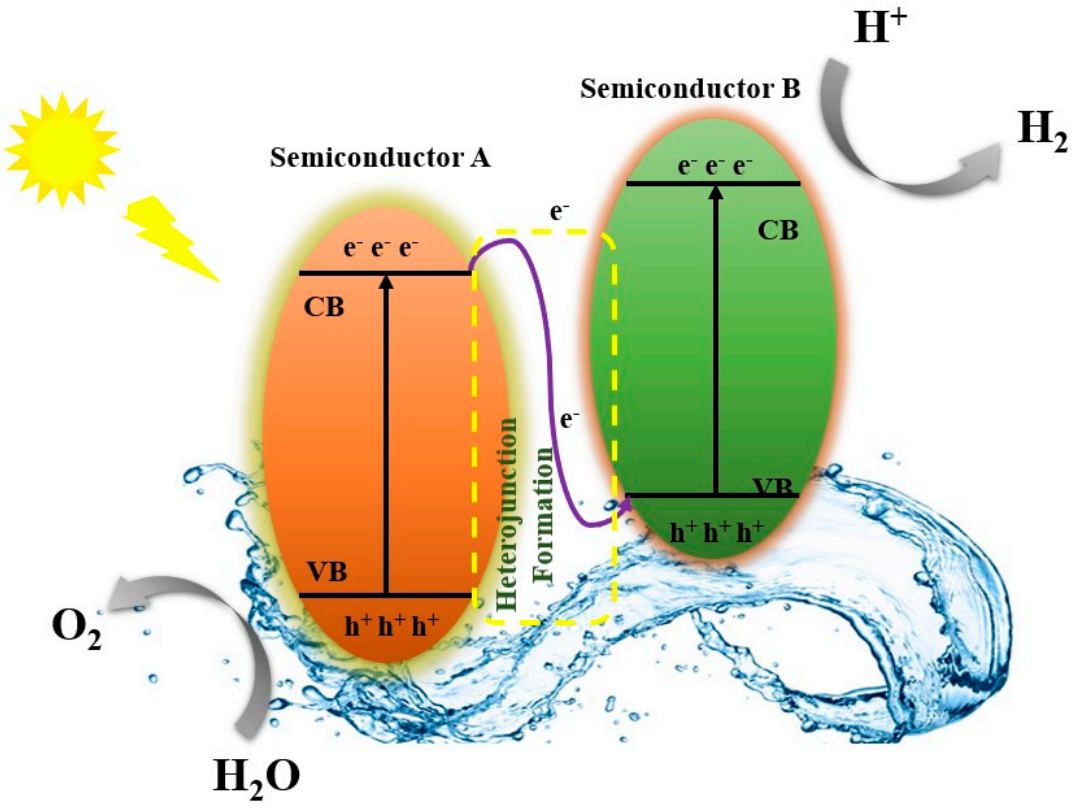


Figure 2. Schematic diagram of two different semiconductors showing heterojunction formation.

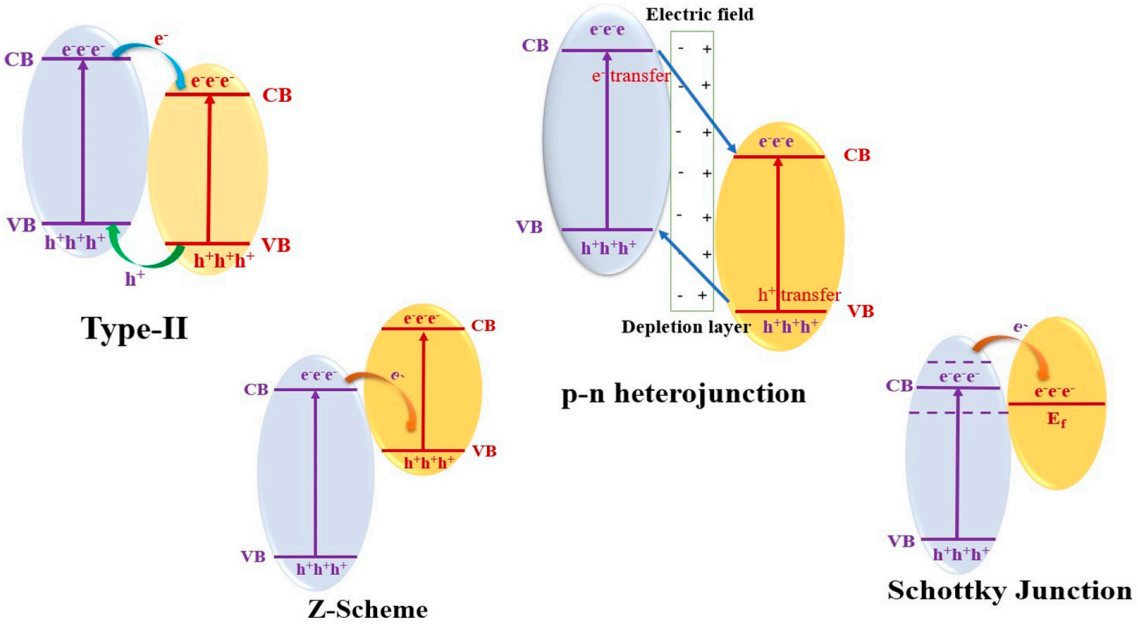


Figure 3. Schematic diagram of different types of heterojunctions.

3.1. Type II Heterojunctions

Type II heterojunctions are also known as staggered band systems due to the staggered alignment of bands between the two semiconductors [51]. The electrons transfer from the semiconductor with the higher CB to the semiconductor with the lower CB, and holes transfer from the semiconductor with the lower VB to the higher VB of the second semiconductor, respectively. In a type II heterojunction, electrons and holes migrate in opposite directions. Apart from type II, there are also type I and type III heterojunctions. Type I has a straddling band alignment, and type III is of broken band type. However, the type II heterojunction is the most promising for water splitting as it facilitates the effective separation of electron–hole pairs [52]. $V_2O_5/BiVO_4$ [53], $BiVO_4/TiO_2$/FTO [54], and $BiVO_4/CeO_2$ [55] are some of the Bi-based type II heterojunctions for feasible OWS applications. Yaw et al. [53] synthesized $V_2O_5/BiVO_4$ type II heterojunction photoelectrodes for PEC applications. Cheng et al. [54] synthesized a ternary type II heterostructured photocatalyst $BiVO_4/TiO_2$/FTO by constructing $BiVO_4$ on fluorine-doped tin oxide (FTO) and TiO_2, improving the charge separation ability of the catalyst. Wetchakun et al. [55] synthesized $BiVO_4/CeO_2$ type II heterojunction photocatalysts through hydrothermal synthesis. These are the few catalytically optimized type II heterostructured systems in Bi-based oxides.

3.2. Z-Scheme Heterojunctions

These can be classified into traditional and direct Z-scheme heterojunctions. In the traditional Z-scheme, there is a redox mediator that works as the charge carrier. It was proposed by Bard in 1979, and it improves charge separation efficiency and shows great redox ability. However, the major disadvantages of this method are that it is only confined to the solution phase and is prone to pH sensitivity and undesirable side reactions. While in the case of the direct Z-scheme, no intermediate is usually employed. This heterojunction is analogous with natural photosynthesis and exhibits high electron–hole separation propensity and redox ability [35,56]. In 2006, Tada et al. [57] introduced the solid-state Z-scheme photocatalyst, with two different photocatalytic semiconductors (PS), PS-I and PS-II, and an electron mediator. The two semiconductors must have a suitable band gap for oxidation and reduction potential for the effectual construction of Z-scheme heterojunction. The electrons have high reduction potential, and the holes have a high oxidation potential so that they cannot recombine. In this pathway, electrons and holes recombine at the

interfacial region and possess remarkable redox ability compared with type II heterojunctions. The fabrication cost of Z-scheme heterojunction catalysts is lower than that of type II heterojunctions [58]. Bi_2WO_6/Ta_3N_5, black phosphorus/Bi_2WO_6, $Bi_2WO_6/CuBi_2O_4$, and Bi_2WO_6/Cu_3P are some Bi-based Z-scheme heterojunctions that exhibit enhanced catalytic performance and excellent characteristics towards OWS [59,60]. These Bi-based Z-scheme heterojunctions also possess remarkable responses towards environmental remediation, reported by Dutta et al. [61] who fabricated Z-scheme $BiFeO_3/CuS/SiO_2$ nanocatalysts for the degradation of methyl orange dye. Ternary Z-scheme systems deliver an effective pathway for the separation of photogenerated electron–hole pair by maintaining the redox potential and possessing excellent visible light-driven PC and PEC activities [62].

3.3. p–n Heterojunctions

The diffusion of charge carriers between two different semiconductors, specifically p- and n-type materials, develops an internal electrical field (IEF) ascribed to the distribution of electrons and holes in the heterojunction. This space charge region is known as a p–n heterojunction [63]. IEF emerges between Bi-based heterostructures during p–n heterojunction formation and infers the advanced catalytic efficiency towards overall water splitting [63–69]. Apart from p–n heterojunctions, there are also n–n type (consists of both n-type) semiconductors and p–p type (containing both p-type) semiconductors. Charge separation is faster in p–n type compared to the p–p type and n–n type heterojunctions [67]. The various Bi-based p–n heterojunctions such as Bi_2WO_6/BiOI [63], BiOBr/Bi_2WO_6 [64], and BiOCl/$BiVO_4$ [65] have been exploited to increase the catalytic efficiencies of pristine Bi-based compounds. Bi_2MoO_6 is an n-type semiconductor that forms a heterojunction with p-type Ag_2O, creating an Ag_2O/Bi_2MoO_6 p–n heterojunction [66]. Dai et al. [63] synthesized a $BiOI/TiO_2$ p–n junction by coating BiOI on TiO_2 through the hydroxylation method. BiOCl is a p-type semiconductor with a wide band gap of ~3.5 eV and exhibits negligible catalytic activity. Feng et al. [65] doped it with $BiVO_4$ to engineer a BiOCl/$BiVO_4$ p–n heterojunction which exhibited marvelous photocatalytic activity. Peng et al. [69] synthesized Bi_2O_3/Bi_2WO_6 p–n heterojunctions with enhanced charge separation. $BiFeO_3$ is a single perovskite photocatalyst with a band gap of ~2.1 eV that shows multiferroic properties, due to which Arunkumar et al. [70] fabricated $BiFeO_3/SnS_2$ p–n heterojunctions for pollutant degradation. The separation of photogenerated electron–hole charge carriers is thermodynamically attainable because the CB and the VB in p-type semiconductors are higher than those in n-type semiconductors, thus forming p–n heterojunctions. The charge carrier separation in p–n heterojunctions is faster than that of type II heterojunction photocatalysts due to the synergistic effect of IEF and band alignment [71].

3.4. Schottky Heterojunctions

This is the junction formed between a semiconductor and a metal. Due to unequal Fermi energy levels, a Schottky barrier is formed, which helps subdue the back recombination of photogenerated electron–hole pairs. In Schottky heterojunctions, the electrons are transferred from the surface plasmon of metal with higher work function (ϕ) to the semiconductor with lower ϕ or excited electrons from semiconductor to metal. Mainly, metals with high ϕ are doped with n-type semiconductors to form a Schottky junction. Various noble metals such as Pt, Pd, Au, and Ag are incorporated in Bi-based compounds to enhance their catalytic efficiency [72]. The synergistic effect of the metal nanoparticles on the surface of the semiconductor enhances the separation of the charge carriers [73]. In the past decade, various Bi-based Schottky heterojunction catalysts have been employed for OWS applications, such as Ag/Bi_3TaO_7 [72], Pt/Bi_2WO_6 [73], Ag/Bi_2S_3 [74], and $Ag/BiVO_4$ [75].

4. Bi-Based Heterostructures Exploited in Multi-Functional H_2 Generation

The synthesis of Bi-based heterostructures has made consistent improvement, and several advanced synthetic strategies have been developed and engaged in designing Bi-based heterostructures with distinct nanostructures. The conventional features of all the synthetic routes are to upgrade the physiochemical properties and to produce a significant number of catalytically active sites. As a result, to achieve nanocatalysts propelled by morphology and surface area, it is important to employ modern synthetic approaches such as solvothermal/hydrothermal methods [76–79], the polymeric citrate precursor (PCP) route [80], the reverse-micellar method [81], the chemical vapor deposition method (CVD) [82], the wet impregnation method [83], and electrochemical methods [84]. The most important Bi-based heterostructured nanocatalysts (Bi_2S_3, Bi_2WO_6, $BiVO_4$, and Bi_2O_3) which yield an excellent catalytic ability with other semiconductors for PC, EC, and PEC applications are studied in detail.

5. Bismuth Sulfite (Bi_2S_3)-Based Heterostructured Nanocatalysts

Bi_2S_3 is an excellent n-type semiconducting material with a distinctive catalytic efficiency and narrow visible range band gap of nearly 1.62 eV, making it an ideally suitable photocatalyst. Bi_2S_3 exhibits an excellent optoelectronic property, a high absorption coefficient of 10^4–10^5 cm^{-1}, and lesser toxicity [85], due to which pristine Bi_2S_3 and its heterostructures have been used in diverse photocatalytic applications such as solar cells [86], lithium-ion batteries [87], photodetectors [88], etc. Different morphologies of Bi_2S_3 nanostructures can be attained depending on various physicochemical parameters such as temperature, solvent system, and surfactant [89]. Among the conventional chemical routes generally employed, the hydrothermal method is by far the most versatile procedure for the fabrication of Bi_2S_3 nanorods [90], nanoflowers [91], and nanotubes [92]. Despite possessing tailored band energy, Bi_2S_3 has certain disadvantages, such as photocorrosiveness and rapid back recombination of charge carriers during photocatalytic water splitting [93]. Bi_2S_3 forms effective heterojunctions with $BiVO_4$ [94], MoS_2 [95], CdS [96], TiO_2 [97], and ZnS/ZnO [98] for efficient H_2 generation via OWS. Mahadik et al. [94] synthesized $Bi_2S_3/BiVO_4$ through a PEC transformation approach, which had an enhanced optoelectronic property due to the synergistic effect between Bi_2S_3 and $BiVO_4$. It exhibited a remarkable photocurrent density of 3.3 mA cm^{-2} at 0.67 V potential, and an H_2 production rate of ~417 μmol cm^{-2} h^{-1}. Zhou et al. [95] fabricated Bi_2S_3/MoS_2 heterostructured electrocatalysts through a hydrothermal method which exhibited a lowered overpotential (η) of 124 mV and a Tafel slope of 123 mV dec^{-1} at the current density of 10 mA cm^{-2}. Bi_2S_3/MoS_2 yielded enhanced HER activity due to the synergistic effect between the two semiconductors in heterojunction with a substantial electrocatalytic surface area. Hao et al. [96] synthesized Bi_2S_3/CdS heterostructure through a sonochemical method for H_2 evolution via photocatalytic OWS. Bare CdS delivered a minimal photocatalytic efficiency of 0.04 mmol h^{-1} g^{-1}. After forming heterojunctions with Bi_2S_3, the H_2 production rate was elevated to 5.5 mmol h^{-1} g^{-1} due to large active sites, unique structure, and effective separation of electron–hole pairs. Ahmad et al. [97] synthesized 3-D rosette–rod TiO_2/Bi_2S_3 heterojunctions, revealing a photocurrent density of 3.98 mA cm^{-2} at 1.23 V. The CB of Bi_2S_3 was found to be more negative than the CB of TiO_2. Hence, electron transfer must have taken place from the CB of Bi_2S_3 to the CB of TiO_2, whereas the holes channeled from the VB of TiO_2 to the VB of Bi_2S_3 and resulted in the movement of electrons and holes in the opposite direction, which ultimately accelerated the charge separation and PEC activity of TiO_2/Bi_2S_3. Sadhasivam et al. [98] synthesized a Bi_2S_3/ZnS/ZnO ternary heterostructure, which depicted enhanced PEC properties and yielded a photocurrent density of 220 $mAcm^{-2}$ at 0.2 V vs. Ag/AgCl. The ternary heterostructure showed higher current density and charge separation efficiency than pristine Bi_2S_3 and Bi_2S_3/ZnO. Wei et al. [99] fabricated ternary $BiVO_4/Bi_2S_3$/NiOOH heterostructures through the electrodeposition of NiOOH over $BiVO_4/Bi_2S_3$ electrodes for evaluating the catalytic efficiency in OWS. $BiVO_4/Bi_2S_3$/NiOOH exhibited a higher photocurrent

density of 0.91 mA cm^{-2} at 1.23 V vs. RHE than that of pristine $BiVO_4$ (0.29 mA cm^{-2} at 1.23 V vs. RHE) and $BiVO_4/Bi_2S_3$ (0.50 mA cm^{-2} at 1.23 V vs. RHE). In the PEC operation, the electrons transferred from the CB of Bi_2S_3 to that of $BiVO_4$ for H_2 production as Bi_2S_3 has more negative CBs and VBs than $BiVO_4$. Bi_2S_3 acted as the light absorber, improving the separation kinetics and transfer of the photo-generated charge carriers. On the one hand, $BiVO_4$ worked as an electron conductor for direct charge transfer to Indium-doped tin oxide glass. On the other hand, NiOOH layers enhanced the PEC activity by providing stability to the $BiVO_4/Bi_2S_3$/NiOOH. Wang et al. [100] fabricated WO_3/Bi_2S_3 through the chemical bath deposition (CBD) method and reported the highest photocurrent density of 5.95 mAcm^{-2} at 1.23 V potential, much higher than that of pristine WO_3 (0.17 mAcm^{-2} at 1.23 V). The enhancement of catalytic activity was observed due to the formation of type II heterojunction that resulted in the easy transport of charge carriers and impeded the rate of back recombination reactions. Subramanyam et al. [101] developed a Bi_2S_3@rGO nanocomposite photoanode for PEC water splitting and yielded a photocurrent density of 6.06 mA cm^{-2} at 1.23 V and higher H_2 generation efficiency of 68.5 µmol/h due to the synergistic effect between Bi_2S_3 and rGO. The mechanism of electron transfer in Bi_2S_3@rGO for PEC water splitting is depicted in Figure 4. These are some remarkable recent reports of Bi_2S_3-based heterostructures, which revealed their catalytic efficiency in H_2 production via OWS.

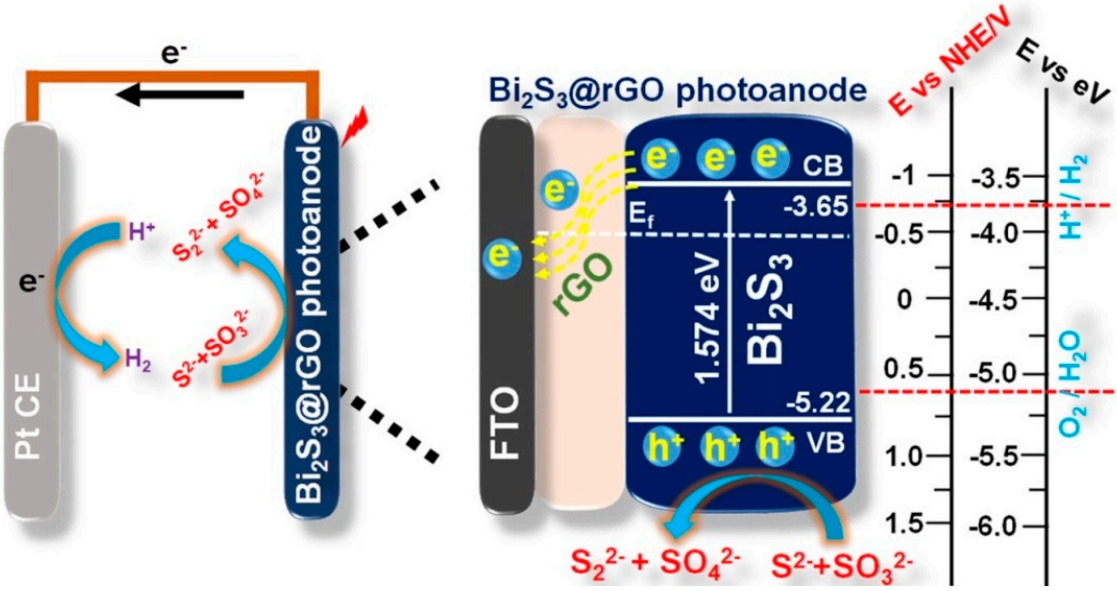


Figure 4. Schematic charge-transfer process in the Bi_2S_3@rGO composite photoanode under light illumination. [Reprinted with permission from reference [101]. Copyright 2021, American Chemical Society].

6. Bismuth Tungstate (Bi_2WO_6)-Based Heterostructured Nanocatalysts

Bi_2WO_6 is a cost-efficient, chemically stable, and environmentally benign Bi oxide with an Aurivillius phase perovskite structure composed of layers between $[Bi_2O_2]^{2+}$ and WO_6. The Bi_2WO_6 has a narrow band gap of ~2.8 eV, and its band contains 2p, 6s, and 5d orbitals of O, Bi, and W, respectively [33]. Monolayer Bi_2WO_6 exhibits excellent catalytic efficiency for green H_2 production via OWS [102]. Bi_2WO_6 can be synthesized through various methods such as hydrothermal, solvothermal, microemulsion, sol–gel, and co-precipitation routes [103–105]. Despite its visible light-driven band energy, certain constraints impede its catalytic activity, such as the back recombination of electrons and sluggish kinetic reaction barriers in PC, PEC, and EC. Therefore, to obtain a higher efficiency via interfacial charge transfer, Bi_2WO_6 forms heterojunctions with BiO [106], Bi_2O_3 [107], $BiVO_4$ [108], $AgInS_2$ [109], $ZnIn_2S_4$ [34], TiO_2 [110], and graphene [111]. Parnicka et al. [109] developed

$AgInS_2/Bi_2WO_6$ via a deposition method. The band energy of both semiconductors was well matched and resulted in an effective heterojunction for higher efficiency. Upon visible light irradiation, the electrons from the CB of Bi_2WO_6 combined with the holes in the VB of $AgInS_2$. In contrast, the holes and electrons from the more positive VB of Bi_2WO_6 and the more negative CB of $AgInS_2$, respectively, participate in oxidation and reduction reactions, respectively, as shown in Figure 5a,b. This increases the charge separation as well as the redox ability. The synthesized $AgInS_2/Bi_2WO_6$ depicts a small decrease after reuse and slight decline in activity after three months; furthermore, there were no structural changes confirmed by XRD analysis which showed the stability and reusability of the nanocatalysts, as shown in Figure 5c–e. $AgInS_2/Bi_2WO_6$ showed the optimum H_2 production rate of 152.75 μmol g^{-1} h^{-1}, which is much higher than pristine Bi_2WO_6, as shown in Figure 5f. The hydrothermal method is a proven approach for synthesizing nanocatalysts [112]. Xiong et al. [113] proposed Z-scheme BP/monolayer Bi_2WO_6 heterojunctions for an efficient charge separation through the hydrothermal method. Black phosphorous (BP) has high charge mobility, tunability, and variant characteristics, and a high surface area. BP is an excellent catalyst for HER and OER in water splitting [114]. The CB and VB energies of BP are −0.8 V and 0.7 V, respectively. BP/Bi_2WO_6 had an H_2 evolution rate of 21,042 μmol/g with Pt as a cocatalyst, and triethanolamine as a hole sacrificial agent, which is 9.15 times higher than that of pure monolayer Bi_2WO_6. The graphene-based Bi_2WO_6 heterostructures are prepared through the hydrothermal method [115]. As reported, a single layer of Bi_2WO_6 shows a significant H_2 generation (5.6 μmol g^{-1} h^{-1}), which showed a 14 times enhanced rate than that of bulk Bi_2WO_6 [116]. Two-dimensional materials exhibit vast applications due to their superior surface area and improved charge separation. Two-dimensional Bi_2WO_6 fabricated with the CTAB-assisted hydrothermal method revealed an excellent photocatalytic activity compared with its single monolayer counterpart [117]. Zhao et al. [118] synthesized Bi_2WO_6/RGO (reduced graphene oxide) nanocomposite through the electrospinning method with an H_2 production efficiency of ~935 μmol h^{-1}, much higher than that of Bi_2WO_6. RGO has an exceptional ability to accept and transfer electrons, but an excess amount of it can decrease the photocatalytic activity. The electrons on the CB of Bi_2WO_6 transferred through RGO, thus improving the separation efficiency of the photogenerated charge carriers. Arif et al. [119] fabricated Z-scheme Bi_2WO_6/CdS heterostructures with a two-step hydrothermal method. CdS has a band gap of ~2.4 eV, showing an enhanced optoelectronic property for water splitting [120]. The VB and CB of CdS are well matched with Bi_2WO_6 for constructing heterojunctions. Bi_2WO_6/CdS heterostructures fabricated with the H_2 evolution of ~167 mmol h^{-1} and Pt loaded showed an increased H_2 efficiency of ~1223 mmol h^{-1}, as Pt is a very promising co-catalyst for the generation of H_2, and has a low overpotential and electron accepting ability. Chachvalvutikul et al. [34] constructed Z-scheme $Bi_2WO_6/ZnIn_2S_4$ heterostructured nanocatalysts via the hydrothermal method, using methanol as a sacrificial agent. The photocatalytic H_2 production rate of $Bi_2WO_6/ZnIn_2S_4$ at different compositions was measured, and the highest reported rate was found to be 395.5 μmol $h^{-1}g^{-1}$ at 12.5% $Bi_2WO_6/ZnIn_2S_4$, as shown in Figure 6a. The catalyst showed excellent reusability and stability after three successive runs, as depicted in Figure 6b. Upon irradiation, the electrons and holes were produced in the CB and VB of both the semiconductors, then the electrons in the CB of $ZnIn_2S_4$ channeled towards the CB of Bi_2WO_6, and the holes in the VB of Bi_2WO_6 streamed towards the VB of $ZnIn_2S_4$, as depicted in Figure 6c.

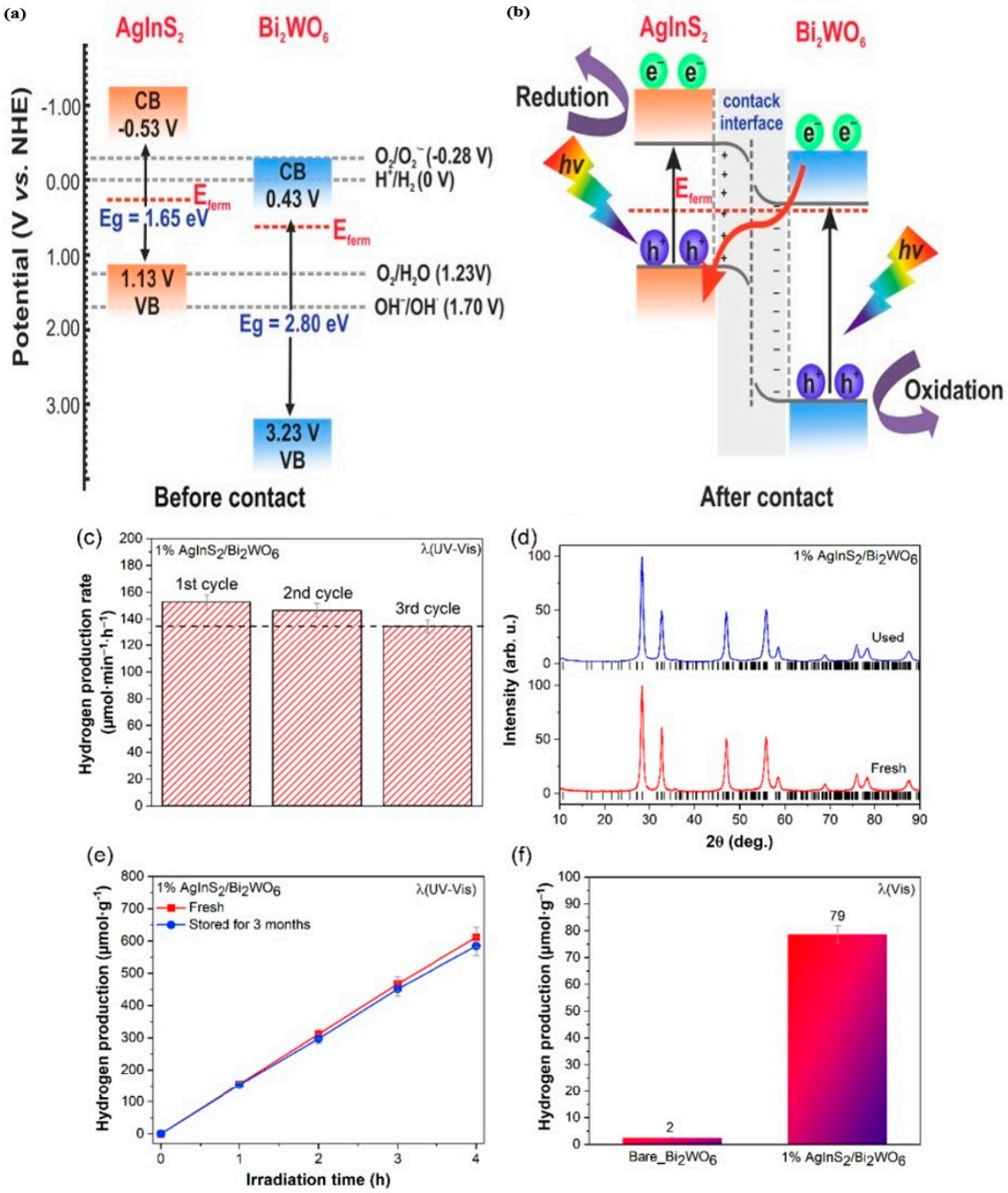


Figure 5. (**a**,**b**) Schematics for band gap match and electron–hole pair separation in $AgInS_2$ QDs/Bi_2WO_6 composite (before/after contact), (**c**) Reusability, (**d**) XRD pattern of 1 wt% $AgInS_2$-modified Bi_2WO_6 before/after three cycles of PC-H_2 generation, (**e**) Stability during prolonged storage of 1 wt% $AgInS_2$-modified Bi_2WO_6, and (**f**) Visible light irradiation in presence of $AgInS_2/Bi_2WO_6$. [Reprinted with permission from reference [109]. Copyright 2020, Elsevier].

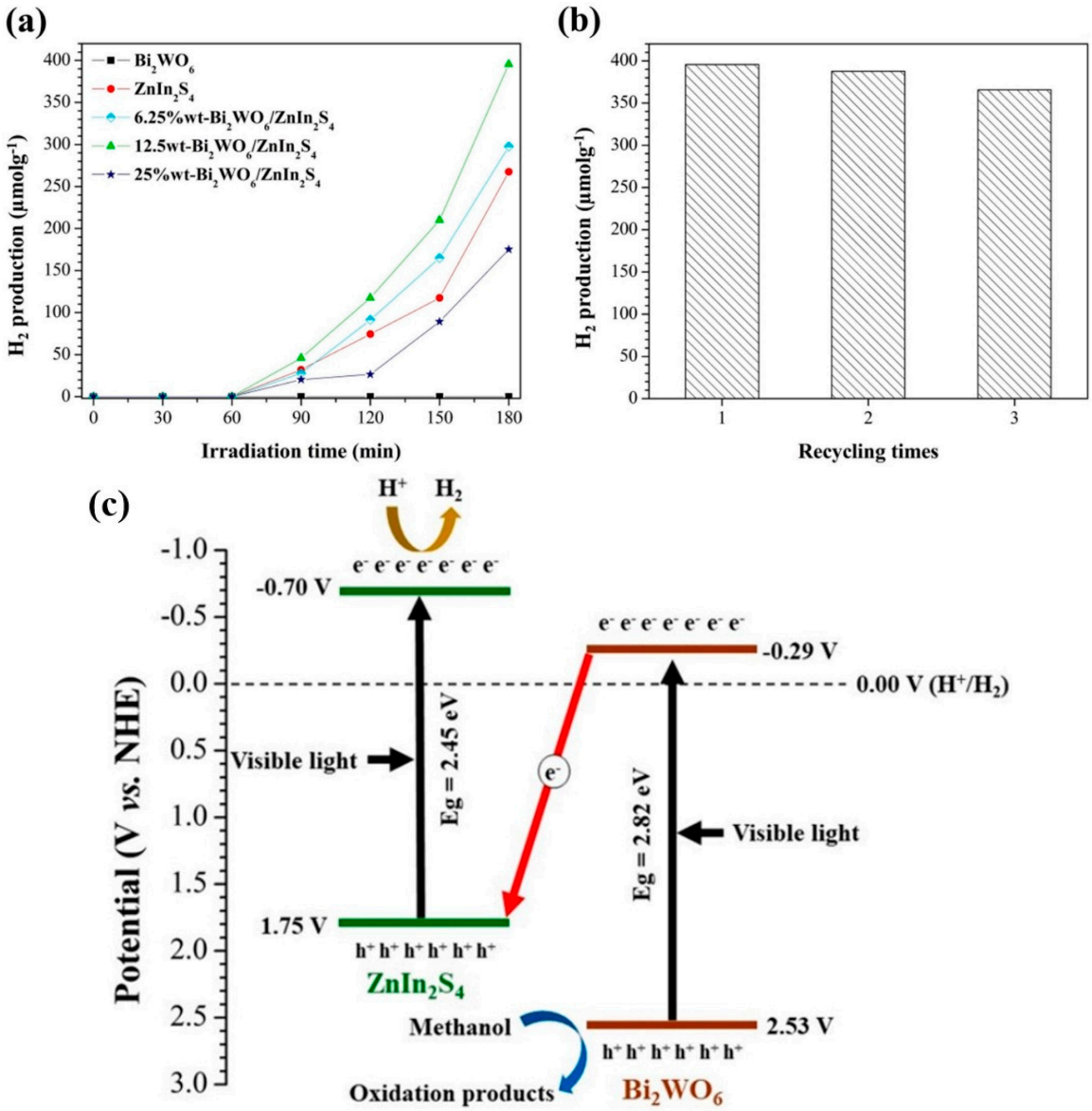


Figure 6. (**a**) Photocatalytic H_2 production of $Bi_2WO_6/ZnIn_2S_4$ with different amount of Bi_2WO_6 in comparison with the Bi_2WO_6 and $ZnIn_2S_4$ photocatalysts, (**b**) Cyclic H_2 production on 12.5%wt $Bi_2WO_6/ZnIn_2S_4$, and (**c**) Charge transfer mechanism for H_2 production by $Bi_2WO_6/ZnIn_2S_4$ heterojunction. [Reprinted with permission from reference [34]. Copyright 2021, Elsevier].

7. Bismuth Vanadate ($BiVO_4$) Based Heterostructured Nanocatalysts

This is an n-type semiconductor with a band gap of 2.4 eV, with controlled morphology. It is a very promising nanocatalyst with low toxicity, higher stability towards photo-corrosion, low cost, and excellent photocatalytic activity with a narrow visible range. $BiVO_4$ exists in different polymorphic forms, which are tetragonal zircon, tetragonal scheelite, and monoclinic scheelite [121]. The reported solar energy efficiency of pristine $BiVO_4$ is about 9%, and its photocurrent density is 6.47 mA cm^{-2} at 1.23 V vs. Ag/AgCl [122]. Kudo et al. [27] reported $BiVO_4$ for water oxidation in 1998 for the very first time. $BiVO_4$ has certain disadvantages such as low charge separation efficiency and poor transport ability. To enhance its catalytic efficiency, $BiVO_4$ forms heterojunctions with $ZnIn_2S_4$ [35], Fe_2O_3 [123], V_2O_5 [52], BP [124], and WO_3 [125]. Xia et al. [123] constructed $Fe_2O_3/BiVO_4$ photoanodes with a higher H_2 production of ~28 μmol cm^{-2} h^{-1} through the spin-coating successive ionic layer adsorption and reaction (SILAR) method, which is considerably higher than that of bare $BiVO_4$ photoanode. $Fe_2O_3/BiVO_4$ photoanode

exhibited a photocurrent density of 1.63 mA cm^{-2} at 1.23 V vs. RHE, and is considered an excellent catalyst for PC and PEC applications. Yaw et al. [53] synthesized $V_2O_5/BiVO_4$ type II heterojunctions through a facile electrodeposition method with a current density of 1.53 mA cm^{-2} at 1.5 V vs. Ag/AgCl, a much improved efficiency than that of individual V_2O_5 (0.21 mA cm^{-2}) and $BiVO_4$ (0.22 mA cm^{-2}). WO_3 is an n-type semiconductor with a band gap of ~2.5–2.8 eV. It is stable at a low pH and shows a higher catalytic efficiency than that of TiO_2 [126]. Sitaaraman et al. [125] synthesized $WO_3/BiVO_4$ heterostructures through spin coating and studied them for PEC applications. WO_3 has a low pH and a greater H_2 generation efficiency. The VB of WO_3 is positive for the oxidation of H_2O, whereas the CB is not negative enough for H_2 generation. Thus, during PEC water splitting, O_2 can be produced easily but H_2 cannot and requires an external potential. Therefore, WO_3 forms a heterojunction with another n-type semiconductor to produce both H_2 and O_2 at the respective sites. Kalanoor et al. [127] reported Mo-doped $WO_3/BiVO_4$ and showed a high photocurrent density of ~1.48 mA/cm^2 with high PEC applicability. Baek et al. [38] introduced $BiVO_4/WO_3/SnO_2$ ternary heterojunctions with improved charge transport and a photocurrent density of ~3.1 mA/cm^2. Combining SnO_2 with $BiVO_4/WO_3$ promoted electron transfer and the separation of charge carriers. The photoelectrocatalyst showed higher efficiency and fabricated type II heterojunctions using the sol–gel method. It is a triple-layer photoanode with improved charge separation. The structural and morphological analysis helped characterize the different layers. $ZnIn_2S_4$ is an excellent photocatalyst due to its remarkable energy band structure and outstanding optoelectronic properties, as discussed above. Hu et al. [35] synthesized $ZnIn_2S_4/BiVO_4$ through a self-assembly method. $ZnIn_2S_4$ has a smaller work function ϕ (3.54 eV) and a higher Fermi level. It forms type II heterojunctions with $BiVO_4$, which exhibits a higher ϕ (4.69 eV) and a lower Fermi level. The electrons migrate from the CB of $BiVO_4$, while holes remain in the VB, as displayed in Figure 7. ZIS/BVO heterostructured nanocatalysts infer the improved photocatalytic activity with an H_2 evolution of ~5944 μmol h^{-1} g^{-1} and stability over four consecutive cycles, as demonstrated in Figure 8. V_2O_5 is an n-type semiconductor with a band gap of 2.3 eV. Yaw et al. [128] synthesized $V_2O_5/RGO/BiVO_4$ through the electrodeposition method. It is a type II heterojunction with a photocurrent density of 2.1 mAcm^{-2} at 1.5 V vs. Ag/AgCl, which is higher than that for pristine $BiVO_4$ (0.22 mAcm^{-2}). On visible light irradiation, the electrons migrate from the CB of $BiVO_4$ to the CB of V_2O_5 for the H^+/H_2 reaction, while holes migrate to evolve O_2. RGO has a high conductivity and higher charge mobility of photogenerated charge carriers, thus designing its ternary heterostructure with $V_2O_5/BiVO_4$ corroborating the high PEC performance. Optimized $V_2O_5/RGO/BiVO_4$ heterojunction photoanodes show a higher H_2 generation efficiency of ~32.7 mmol/h.

Majumder et al. [129] fabricated $BiVO_4/Bi_2S_3/NiCoO_2$ ternary heterostructured catalysts for PEC water splitting through the electrodeposition method with the maximum photocurrent density of 3.80 mA cm^{-2} (at 1.23 V vs. RHE), higher than that for $BiVO_4/Bi_2S_3$ and $BiVO_4$, which achieved 3.39 mA cm^{-2} and 2.49 mA cm^{-2} (at 1.23 V vs. RHE) photocurrent density, respectively. $NiCoO_2$ is a p-type semiconductor. $BiVO_4/Bi_2S_3/NiCoO_2$ formed n–n–p type heterojunctions, as depicted in Figure 9. Fang et al. [130] discussed the advantages of $NiCoO_2$ as the efficient co-catalytic system in $BiVO_4$-led catalysis. Ni–Co oxides possess remarkable active surface area for an electrochemical reaction and show significant stability. The tetrahedral sites in $NiCoO_2$ are vacant and provide space for electronic transitions, create more active sites, avoid back recombination, and are cost-effective [130].

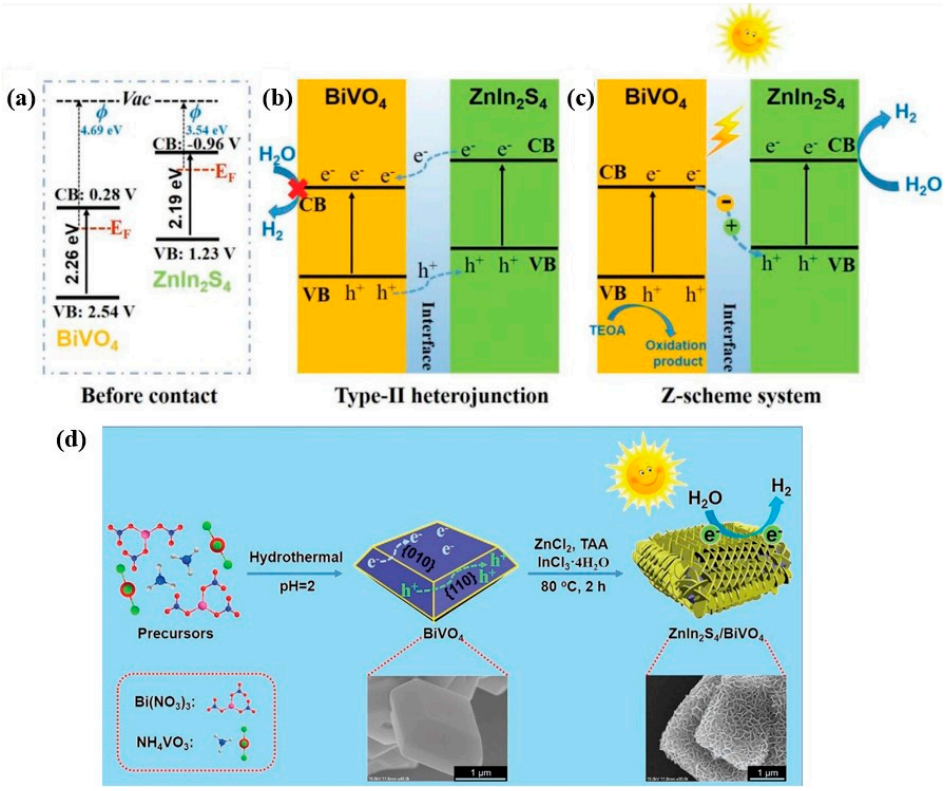


Figure 7. The proposed mechanism of photocatalytic H_2 evolution over ZIS/BVO under visible light irradiation, (**a**) Before contact, (**b**) Type II heterojunction, (**c**) Z-scheme system, and (**d**) Schematic diagram showing the synthesis of ZIS/BVO heterojunction. [Reprinted with permission from reference [35]. Copyright 2020, John Wiley and Sons].

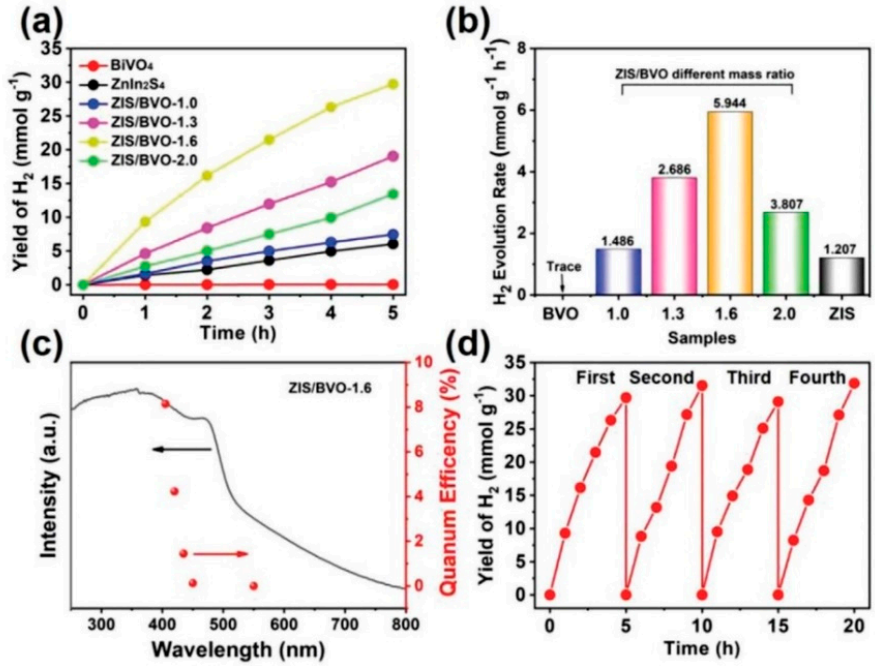


Figure 8. (**a**,**b**) Photocatalytic H_2 evolution performance of the prepared samples, (**c**) Wavelength dependence of quantum H_2 evolution efficiency of ZIS/BVO-1.6, and (**d**) Multiple cycles of H_2 production over ZIS/BVO-1.6. [Reprinted with permission from reference [35]. Copyright 2020, John Wiley and Sons].

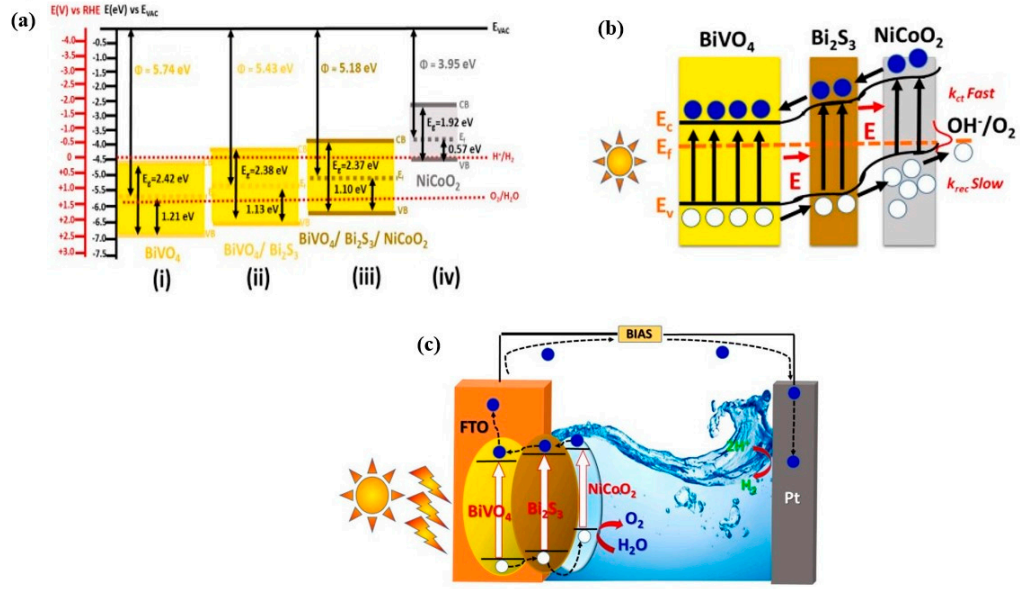


Figure 9. (**a**) Estimation of the band alignment calculated from UPS analysis with regard to vacuum and converted to E (V) vs. RHE, whereas (**b**) shows the schematic of n–n–p junction ladder in the staggered band structure of $BiVO_4/Bi_2S_3/NiCoO_2$ photoanode. The terms k_{rec} and k_{ct} refer to the surface recombination and charge transfer through surface states, respectively, and (**c**) shows the schematic of the water oxidation of $BiVO_4/Bi_2S_3/NiCoO_2$ photoanode. [Reprinted with permission from reference [129]. Copyright 2022, Elsevier].

8. Bismuth Oxide (Bi_2O_3)-Based Heterostructured Nanocatalysts

Bi_2O_3 is considered an excellent semiconductor with a band gap of 2.6–2.8 eV, has high active surface area, and exhibits enhanced catalytic efficiency for OWS. Various heterostructures have been fabricated to improve the photocatalytic performances of Bi_2O_3. Bi_2O_3 forms effective heterojunctions with Bi_2SiO_5 [131], Bi_2WO_6 [107], Bi_2MoO_6 [132], $BiVO_4$ [133], and MoS_2 [134]. Goud et al. [134] fabricated MoS_2/Bi_2O_3 through the hydrothermal method. MoS_2 has a band gap of 1.93 eV and a HER efficiency of the order of platinum, along with exceptional optoelectronic properties [135]. As the resulted MoS_2/Bi_2O_3 heterojunction has a band gap of 1.61 eV, the decrement in band energy of heterostructured nanocatalysts escalates the photocatalytic activity by enhancing the spectrum of visible light absorption. The H_2 production rate reported for the MoS_2/Bi_2O_3 heterostructured catalyst (3075.21 μmol $g^{-1}h^{-1}$) was found to be nearly 7-fold higher than that of MoS_2 (428.14 μmol $g^{-1}h^{-1}$). The photocatalytic activity of MoS_2/Bi_2O_3 was also evaluated with a different hole scavenger for an efficient electron transfer, as shown in Figure 10a. The photocurrent response investigated for different compositions of MoS_2/Bi_2O_3 and pristine MoS_2 and Bi_2O_3 is illustrated in Figure 10b. Analogous to Bi_2WO_6, Bi_2MoO_6 is also an important Bi-based perovskite structure [136], with layers between $[Bi_2O_2]^{2+}$ and $[MoO_4]^{2-}$. Various modification strategies have been developed to improve the photocatalytic activity of Bi_2MoO_6, which has an optical band energy of 2.7 eV. Bi_2MoO_6 has a layered structure with enormous potential for CO_2 reduction, H_2 generation, O_2 generation, pollutant degradation, and many more environmental applications [137,138]. However, the efficiency of this single component photocatalyst is restricted due to rapid charge carrier recombination and slow charge transportation. To enhance its catalytic activity, Bi_2Mo_6 forms heterostructures with different semiconductors [139,140]. Fu et al. [132] synthesized Bi_2O_3/Bi_2MoO_6 Z-scheme heterojunctions yielding a 96.4% degradation efficiency, and the higher photocatalytic H_2 evolution rate of 12.97 μmol $h^{-1}g^{-1}$ in visible light irradiation. Chao et al. [107] synthesized Bi_2O_3-Bi_2WO_6 p–n heterostructured nanocatalysts through the solvothermal method. The results highlighted that Bi_2O_3-Bi_2WO_6 formed p–n heterojunctions as they have a more positive VB than needed for the oxidation potential and have

more negative CB than needed for the reduction potential, as shown in Figure 11a, and it exhibited the highest photocatalytic efficiency of 878 μmol h^{-1} g^{-1}, along with a marvelous durability, which was confirmed by performing three cycles, as revealed in Figure 11b. Ye et al. [141] synthesized $Bi_2O_3/BiVO_4$ p–n heterojunctions through the hydrothermal method with the improved photoelectrocatalytic activity. It yielded a maximum photocurrent density of 2.58 mA cm^{-2} at 1.2 V vs. Ag/AgCl. Shafiq et al. [133] also fabricated $Bi_2O_3/BiVO_4$ heterojunctions and reported their photocatalytic activity for H_2 production, which was found to be as high as 171.13 μmol h^{-1} g^{-1}. This response was markedly higher than the performance of individual Bi_2O_3 and $BiVO_4$ semiconductor nanocatalysts. Salomao et al. [142] fabricated $ZnBi_{38}O_{60}/Bi_2O_3$ with increased surface area and a photocurrent density of −1.55 mA cm^{-2} with 100% H_2 generation efficiency. Syah et al. [143] synthesized Bi/Bi_2O_3 on Ni-foam electrocatalysts, exhibiting high surface area, higher mobility, and an effective transportation of electrons. Bi/Bi_2O_3 on Ni-foam yielded a high photocurrent density, low overpotential, and excellent robustness. Salomao et al. [144] designed ternary heterostructures of $Bi_2O_3/Al_2Bi_{24}O_{39}/Al_2Bi_{48}O_{75}$ (Bi_2O_3/BiAl) nanowires through a spray pyrolysis method with the suitable VB and CB for redox reactions towards water splitting. They show the highest photocurrent density of −4.85 mA cm^{-2} at 0 V vs. RHE with H_2 evolution of 348 μmol/cm^2/h and 93% faradaic efficiency.

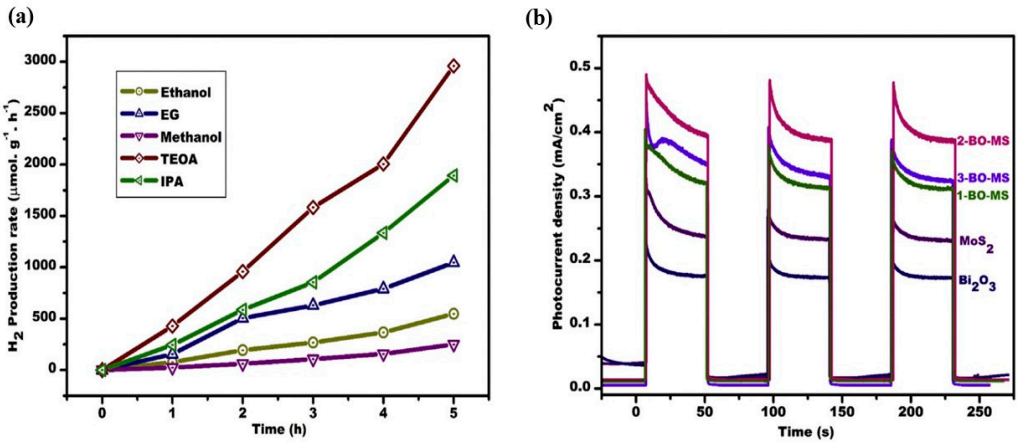


Figure 10. (**a**) Photocatalytic H_2 evolution rate over various scavengers, (**b**) Photocurrent response of the MoS_2, Bi_2O_3, 1-BO-MS, 2-BO-MS, and 3-BO-MS catalysts under visible light. [Reprinted with permission from reference [134]. Copyright 2021, Elsevier].

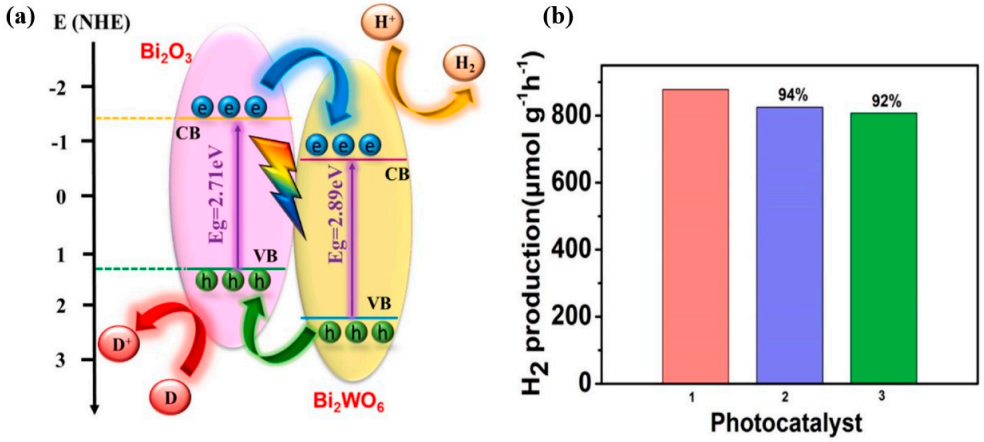


Figure 11. (**a**) Proposed band structures and photocatalysis mechanism of the Bi_2O_3-Bi_2WO_6 photocatalyst and (**b**) cycling tests of photocatalytic H_2 evolution through the BWA400 photocatalyst. [Reprinted with permission from reference [107]. Copyright 2021, Elsevier].

9. Applications

The catalytic efficiency of Bi-based heterostructured nanocatalysts for varied applications in photocatalytic, photoelectrocatalytic, and electrocatalytic H_2 production via water splitting are discussed in this section.

10. Photocatalytic (PC) Water Splitting

The idea of photocatalysis comes from natural photosynthesis, which converts photonic energy into chemical energy [145]. In photocatalytic water splitting, a semiconductor photocatalyst with a narrow band gap and suitable redox potential is required. The principle of photocatalysis is band theory, which consists in continuous energy levels known as Fermi levels. The reduction potential and oxidation potential in electrons and holes depend on the band alignment. Photocatalysts are basically light-harvesting semiconducting materials. Upon visible light irradiation, the very initial step is the excitation of electron–hole pairs; then, the electrons and holes come to the surface of the semiconductor and participate in HER and OER reactions at respective positions, as shown in Figure 12.

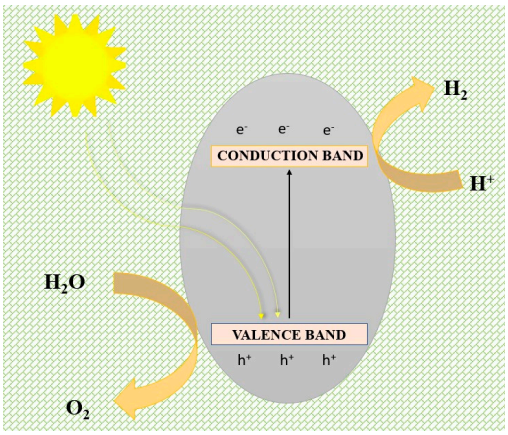


Figure 12. Mechanism of photocatalytic water splitting.

Photocatalytic H_2 generation from water splitting is an environmentally friendly and effective pathway. Generally, in an efficient water splitting process for H_2 generation, there should be an effective interaction between light and catalyst [146]. However, the major challenge in this process is the back recombination of photogenerated charge carriers. Modified heterostructures are well accomplished in improving the photocatalytic efficiency of OWS and are the preferred choice of catalytic systems to deal with back recombination. Bi-based photocatalysts have been studied vastly in the last decade due to their narrow band energies falling in the visible light range, high efficiency, environmentally benign nature, and cost-effectiveness. Li et al. [147] synthesized Bi_2MoO_6/C_3N_4 heterojunctions with the H_2 generation of 563.4 μmol h^{-1} g^{-1} through the solvothermal method. Graphitic carbon nitride (g-C_3N_4) has attracted much attention due to its exceptional catalytic property, low toxicity, high stability, and narrow band gap of 2.7 eV; on the other hand, Bi_2Mo_6 also possesses a narrow band gap of ~2.8 eV. The prepared heterostructures have a high photocatalytic efficiency for H_2 generation as well as for bacterial disinfection. Mei et al. [148] synthesized Bi_2MoO_6/CdSe-diethylenetriamine (DETA) forming Z-scheme heterojunctions through the solvothermal method, with an H_2 production of 5.92 mmol g^{-1} h^{-1}, ascribed to the efficient separation of photogenerated charge carriers. CdSe has a band gap of 1.7 eV, a suitable band for H_2 production. It has adequate active sites for photocatalytic H_2 generation but poor photo-stability, attributed to photo-corrosiveness. Forming Z-scheme heterostructures with Bi_2MoO_6 can improve the stability of CdSe, as well as enhance its photocatalytic activity for H_2 generation. Zhao et al. [149] fabricated $Bi_2Ti_2O_7/g\text{-}C_3N_4/Bi_4Ti_3O_{12}$, a ternary heterostructured photocatalyst, through an electrospinning method with the H_2 evolution of 638 mmol h^{-1} g^{-1}. Samsudin et al. [83]

synthesized $TiO_2/BiVO_4$ via the wet-impregnation method. The heterostructure formation remarkably improved the H_2 production efficiency due to pronounced interfacial charge transfer. Wan et al. [62] fabricated $ZnIn_2S_4$, a $CuOx/Bi_2MoO_6$ photocatalyst via the hydrothermal method. It is a Z-scheme photocatalyst for efficient H_2 and O_2 production via PC water splitting. Pan et al. [26] synthesized $BiPO_4$/RGO through the hydrothermal route, yielding the H_2 production rate of 306 µmol/h/g, which turned out to be nearly 20-fold higher than that of pristine $BiPO_4$ (14.9 mmol h^{-1}). Wu et al. [106] synthesized a Bi_2WO_6-BiO nanocomposite via the hydrothermal method. It showed a desirable H_2 generation efficiency of 73.12 µmol h^{-1} g^{-1} with appropriate VB and CB. Zhao et al. [29] synthesized Bi_2MoO_6/RGO through the electrospinning method. It is a p–n heterojunction with an enhanced H_2 evolution efficiency of 794.7 µmol h^{-1}. Chen et al. [76] fabricated Cr-doped $Bi_4Ti_3O_{12}$ nanosheets via the hydrothermal method. They exhibited an H_2 generation efficiency of 116.75 µmol h^{-1} g^{-1}, which was 2.85 times higher than that of $Bi_4Ti_3O_{12}$. Fu et al. [78] synthesized NiO/Carbon Dots/$BiVO_4$ through the hydrothermal method with an H_2 evolution of 1.21 µmol/h. Guo et al. [28] constructed Sn-doped ZnO/BiOCl via the hydrothermal method. It is an effective Z- scheme heterostructured photocatalyst displaying an H_2 evolution rate of 4146.77 µmol h^{-1} g^{-1}. After going through the aforementioned results, it can be concluded that Bi-based photocatalysts have received an immense interest due to their whopping H_2 production efficiency. Among all the reported photocatalysts, Z-scheme plays an effective role in enhancing the activity of semiconductor photocatalysts. Some of the most important Bi-based heterostructured photocatalysts are demonstrated in Table 1 with their H_2 evolution performance.

Table 1. Photocatalytic efficiency of Bi-based heterostructured nanocatalysts for HER performance.

Nanocatalysts	Type of Heterojunction	Synthesis Method	Photocatalytic H_2 Generation	Ref.
$BiPO_4$/RGO	Type II	Hydrothermal	306 µmol/h/g	[26]
Sn-doped ZnO/BiOCl	Z-scheme	Hydrothermal	4146.77 µmol/h/g	[28]
Bi_2MoO_6/RGO	p–n	Electrospinning	794.7 µmol/h	[29]
$Bi_2WO_6/ZnIn_2S_4$	Z-scheme	Hydrothermal	131.8 µmol/h/g	[34]
$ZnIn_2S_4/BiVO_4$	Z-scheme	Self-assembly	5944 µmol/h/g	[35]
$ZnIn_2S_4$, $CuOx/Bi_2MoO_6$	Z-scheme	Hydrothermal, impregnation method	740.4 µmol/h/g	[62]
Cr-doped $Bi_4Ti_3O_{12}$	Schottky	Sol–gel, hydrothermal	116.75 µmol/h/g	[76]
NiO/CDs/$BiVO_4$	Z-scheme	Hydrothermal	1.21 µmol/h	[78]
$TiO_2/BiVO_4$	Type II	Wet-impregnation method	173 µmol/h/cm^2	[83]
Bi_2S_3/CdS	Type I	Sonochemical method	5.5 mmol/h/g	[96]
Bi_2WO_6-BiO	Type II	Hydrothermal	73.12 µmol/h/g	[106]
Bi_2O_3-Bi_2WO_6	p–n	Solvothermal	878 µmol/g/h	[107]
$AgInS_2/Bi_2WO_6$	p–n	Hydrothermal, hot-injection, deposition treatment	152.75 µmol/g	[109]
TiO_2/Bi_2WO_6	p–n	Electrospinning	11580 µmol/h/g	[110]
Bi_2WO_6-graphene	Type II	Sonochemical method	159.20 mmol/h	[111]
BP/Bi_2WO_6	Z-scheme	Hydrothermal	21042 µmol/g	[113]
Bi_2WO_6/RGO	Type II	Electrospinning	935 µmol/h	[118]
Pt loaded Bi_2WO_6/CdS	Z-scheme	Hydrothermal	1223 mmol/h	[119]
Bi_2WO_6/CdS	Z-scheme	Hydrothermal	167 mmol/h	[119]
$BP/BiVO_4$	Z-scheme	Hydrothermal	160 µmol/h/g	[124]
Bi_2O_3/Bi_2MoO_6	Z-scheme	In situ alkali treatment	12.97 µmol/h/g	[132]
$Bi_2O_3/BiVO_4$	p–n	Electrodeposition	171.13 µmol/h/g	[133]
MoS_2/Bi_2O_3	Z-scheme	Hydrothermal	3075.21 µmol/h/g	[134]
Bi_2MoO_6/g-C_3N_4	p–n	In situ solvothermal	563.4 µmol/h/g	[147]
Bi_2MoO_6/CdSe-DETA	Z-scheme	Solvothermal	5920 µmol/h/g	[148]
$Bi_2Ti_2O_7$/g-C_3N_4/$Bi_4Ti_3O_{12}$	Type II	Electrospinning/calcination	638 µmol/h/g	[149]

11. Photoelectrocatalytic (PEC) Water Splitting

PEC cells consist of a working electrode, reference electrode, and counter electrode and contain an electrode/electrolyte interface, as shown in Figure 13. Water splitting occurs at the surface of the catalyst or at the active sites. Platinum has long been used as the most efficient photoelectrocatalyst for HER due to its binding energy and Gibbs free energy [150]. PEC cells directly convert solar energy to electrical energy. 1.23 eV of energy is required for water splitting. Generally, n-type semiconductors are preferred for photoanode for their better catalytic activity [151]. PEC is developed from PC and EC. Band energy is a very important parameter for selecting a semiconductor photocatalyst for higher efficiency. PEC cells must have a suitable band potential for water splitting; that is, the CB should have more negative reduction potential than H_2. Similarly, VB should have more positive oxidation potential than O_2 [152].

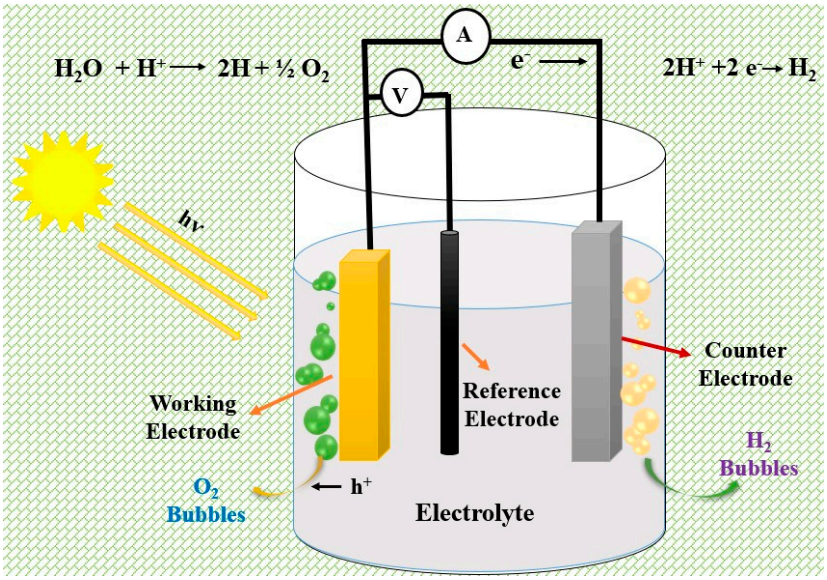


Figure 13. Schematic diagram of photoelectrocatalytic (PEC) water splitting.

In a photo-electrolysis reaction, H_2 and O_2 evolve at the respective photo-electrode by water splitting. PEC water splitting operation does not produce greenhouse gases, and it is a very standard approach to replace H_2 production from fossil derivatives [153]. The various important Bi-based nanocatalysts for PEC are reported in Table 2, with enhanced efficiency towards water splitting. The heterojunction formation enhances the PEC efficiency of the nanocatalysts. It is one of the effective approaches for the separation of charges, and extends the visible absorption region by forming different mechanisms, as discussed above.

Sitaaraman et al. [125] synthesized $BiVO_4$ heterojunctions with tungsten oxide (WO_3). The band gap of WO_3 is ~2.8 eV, and that of $BiVO_4$ is ~2.4 eV. The photocurrent density of the heterostructure was found to be 0.64 mA cm^{-2} at 1.23 V RHE, which was higher than the photocurrent densities of $BiVO_4$ and WO_3. Zeng et al. [154] synthesized cobalt phosphate on WO_3/Mo-$BiVO_4$ through the conventional deposition annealing method, yielding a photocurrent density of 5.38 mA cm^{-2}, with the generation of H_2 and O_2 in the order of 94.7 mmol cm^{-2} h^{-1} and 46.5 mmol cm^{-2} h^{-1}, respectively, suggesting it is a remarkable PEC catalyst for H_2 production, with an IPCE of 81% at 400 nm. Vinoth et al. [155] synthesized Co/S-gC_3N_4/BiOCl heterojunctions through the hydrothermal method. Three-dimensional g-C_3N_4 nanosheets split water into H_2 and O_2 with the higher HER rate of up to 101.4 µmol g^{-1} h^{-1}, which turned out to be much higher than that of bare g-C_3N_4 [156]. Co-doped, S-gC_3N_4/BiOCl type II heterostructured photoanodes exhibited the photocurrent density of 393 µA cm^{-2} at 1.23 V vs. RHE, with enhanced charge separation and electron migration. Wang et al. [157] fabricated $BiVO_4$/FeOOH/NiOOH via the hydrothermal method. It showed a photocurrent density of 5.87 mA cm^{-2} at 1.23 V vs. RHE.

Pilli et al. [158] engineered $WO_3/BiVO_4$/Co-Pi via the electrodeposition method, with a photocurrent density of 6.72 mA cm^{-2} at 1.23 V vs. RHE, and an IPCE of 90% at 450 nm.

Table 2. PEC efficiency of Bi-based heterostructured nanocatalysts for HER performances.

Nanocatalyst	Synthetic Route	Photocurrent Density	H_2 Production	Ref.
$BiVO_4/WO_3/SnO_2$	Sol–gel	3.1 mA cm^{-2} at 1.23 V vs. RHE	-	[38]
$V_2O_5/BiVO_4$	Facile electrodeposition	1.53 $mAcm^{-2}$ at 1.5 V vs. Ag/AgCl	8.2 mmol/h	[53]
$Bi_2S_3/BiVO_4$	PEC transformation	3.3 $mAcm^{-2}$ at 1.23 V vs. Ag/AgCl	417 μmol/cm^2/h	[94]
3-D rosette–rod TiO_2/Bi_2S_3	Hydrothermal	3.98 mA cm^{-2} at 1.23 V vs. RHE	-	[97]
$Bi_2S_3/ZnS/ZnO$	Hydrothermal	220 $mAcm^{-2}$ at 0.2 V vs. Ag/AgCl	-	[98]
$BiVO_4/Bi_2S_3$/NiOOH	Photo-assisted electrodeposition	0.91 mA cm^{-2} at 1.23 V vs. RHE	-	[99]
WO_3/Bi_2S_3	Chemical bath deposition	5.95 $mAcm^{-2}$ at 1.23 V vs. RHE	-	[100]
Bi_2S_3@rGO	Facile-synthetic method	6.06 mA cm^{-2} at 1.23 V vs. RHE, IPCE 15.5% at 475 nm	68.5 μmol/h	[101]
$Fe_2O_3/BiVO_4$	SILAR method	1.63 mA cm^{-2} at 1.23 V vs. Ag/AgCl, IPCE 90% at 450 nm	27.34 μmol/h/cm^2	[123]
$WO_3/BiVO_4$	Spin coating	0.64 $mAcm^{-2}$ at 1.23 V vs. RHE	-	[125]
V_2O_5/RGO/$BiVO_4$	Electrodeposition	2.1 $mAcm^{-2}$ at 1.5 V vs. Ag/AgCl	32.7 mmol/h	[128]
$BiVO_4/Bi_2S_3/NiCoO_2$	Electrodeposition	3.80 mA cm^{-2} at 1.23 V vs. RHE	-	[129]
$Bi_2O_3/BiVO_4$	Hydrothermal	2.58 mA cm^{-2} at 1.2 V vs. Ag/AgCl		[141]
$ZnBi_{38}O_{60}/Bi_2O_3$	Electrodeposition	−1.55 mA cm^{-2} at 0 V vs. RHE	-	[142]

12. Electrocatalytic (EC) Water Splitting

This is a very promising method for green H_2 production. Electrocatalytic water splitting comprises of two reactions: H_2 evolution reaction (HER) at cathode and O_2 evolution reaction (OER) at anode. HER is a two-electron process in an acidic medium, as depicted in Figure 14, whereas OER is a four-electron process. In the electrolysis of water for H_2 production, HER is a key half reaction, whereas OER is a bottleneck for enhancing the OWS due to its sluggish kinetic reactions. Higher potential is needed to overcome the kinetic barrier known as overpotential (η). The major concern for electrocatalytic operation is the high η and large kinetic barriers [159]. For an applicable water splitting reaction, an electrocatalyst with higher activity and desirable stability is required [160]. A current density of 10 mA cm^{-2} is needed to compare the activities of the electrocatalysts, which corresponds to almost 12% of solar energy [161].

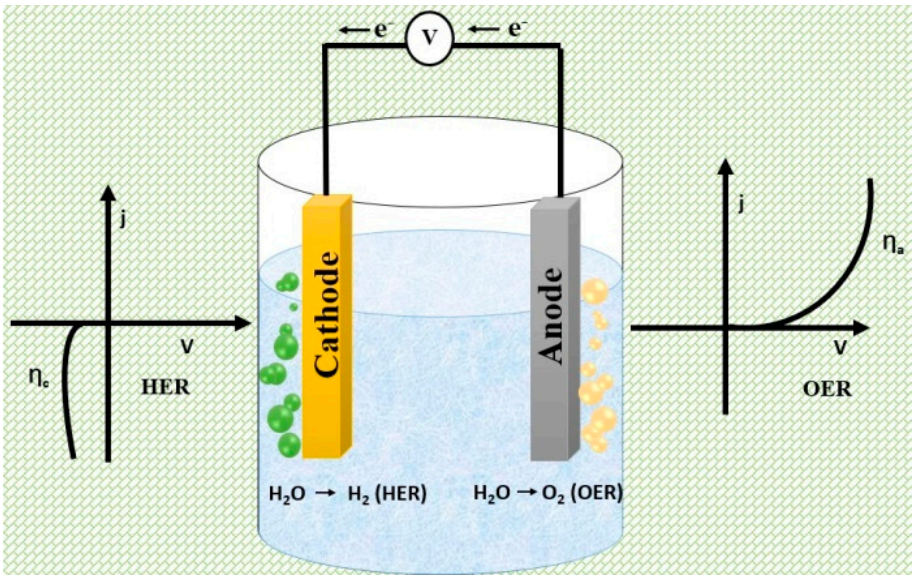


Figure 14. Schematic diagram of electrocatalytic (EC) water splitting.

Electrolysis of water in acidic medium;
Reduction at cathode: $2H^+ + 2e^- \rightarrow 2H_2$
Oxidation at anode: $2H_2O \rightarrow O_2 + 4H^+ + 4e^-$
Overall reaction: $2H_2O \rightarrow H_2 + O_2$

For the above water splitting reaction, 1.23 V electrode potential is required at standard conditions.

Electrocatalysts are important in carrying out effective water splitting applications. The challenge is to develop a catalyst with high durability, low cost, high efficiency, and maximum stability. Electrocatalysts play a significant role in lowering kinetic reactions, and in overcoming kinetic energy barriers. For enhanced activity in an electrocatalyst, a few things need to be addressed; one is conductivity for the better transfer of electrons and the other is favorable electrodes for convenient active sites for better reactions [162,163]. Yang et al. [164] synthesized $MoSe_2/Bi_2Se_3$ through the hot injection method, as depicted in Figure 15c. $MoSe_2$ is a metal dichalcogenide with a narrow band gap of ~1.5 eV, but with poor conductivity. It is used as an energy storage material. On the other hand, Bi_2Se_3 enhances electrochemical efficiency by forming heterojunctions for HER performance [165]. $MoSe_2/Bi_2Se_3$ has a current density of 85 mA cm^{-2}, a low Tafel slope of 44 mV dec^{-1}, and an η of 300 mV, as shown in Figure 15a,b. Khatun et al. [166] synthesized bismuth iron molybdenum oxide (BFMO) composed of Bi_2MoO_6 and $Bi_3(FeO_4)$ $(MoO_4)_2$, which acts as an effective catalyst for both OER and HER reactions. The synthesized electrocatalyst had an excellent electrocatalytic activity towards HER, with an η of 207 mV at current density 10 mA cm^{-2}, and OER, with an η of 266 mV at 10 mA cm^{-2}. It exhibited a potential of 1.67 eV and possessed higher stability, suggesting an excellent electrocatalytic system for OWS.

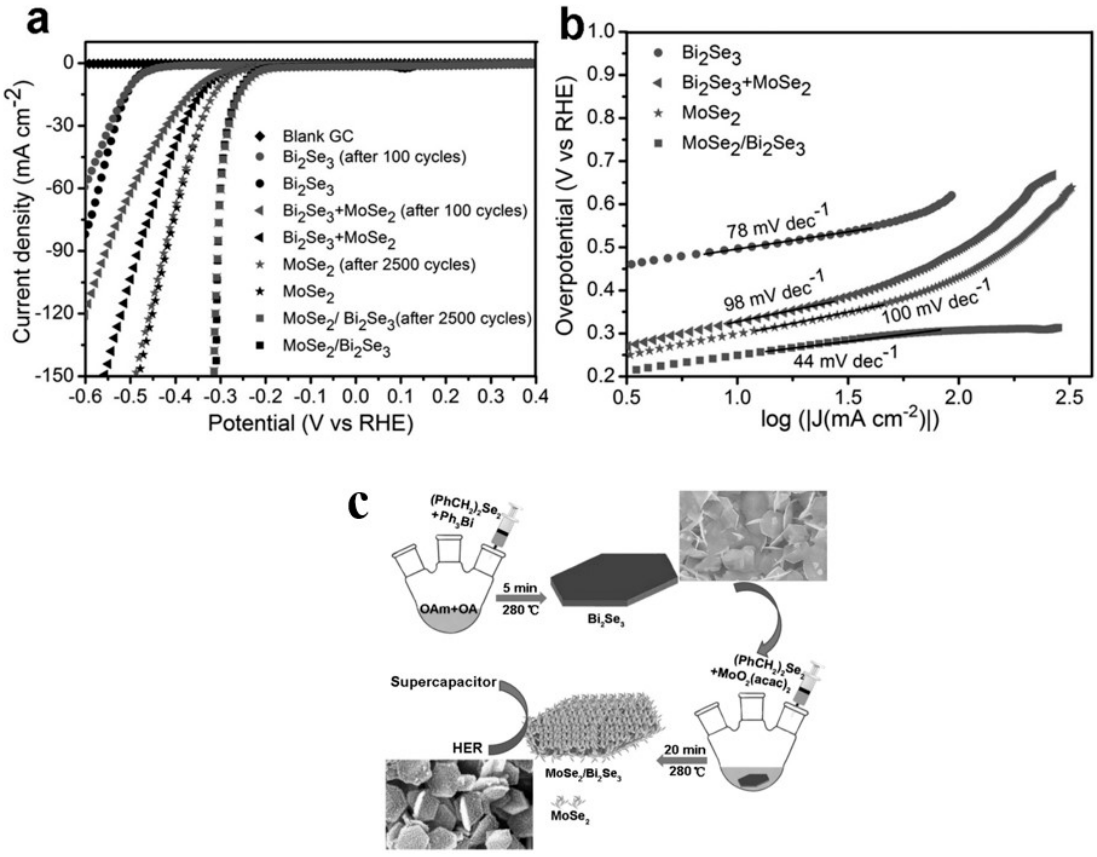


Figure 15. (**a**) Polarization curves, (**b**) Tafel slope, and (**c**) Schematic illustration for synthesis of $MoSe_2/Bi_2Se_3$ hybrids. [Reprinted with permission from reference [164]. Copyright 2017, John Wiley and Sons].

Yang et al. [167] synthesized Bi_2S_3 @CoS_2/MoS_2 with a low Tafel slope of 56.2 mV dec^{-1} and an η of 94.7 mV at 10 mA cm^{-2} of current density. Stability of the electrocatalyst is the basic requirement for water splitting. Razzaque et al. [168] fabricated Bi_2Se_3 nanosheets via the electrochemical method. It showed a Tafel slope of 178 mV dec^{-1} and an η of 220 mV at 10 mA cm^{-2} of current density. Li et al. [169] synthesized Au@Bi_2Se_3 NFs through the hot injection method; it exhibited a Tafel slope of 78 mV dec^{-1} and an η of 375 mV at 10 mA cm^{-2} of current density with an excellent EC activity. The electrochemical systems whose yield accelerate cathodic current density at very low overpotential value are idealized for HER applications [170]. Dileep et al. [171] synthesized $BiSbSe_3$ nanostructure electrocatalysts with a Tafel slope of 178 mV dec^{-1} and an η of 220 mV at 10 mA cm^{-2} of current density. They showed excellent HER activity. The various Bi-based electrocatalysts are listed in Table 3, showing excellent EC activities for HER. There are still challenges left for the construction of an effective electrocatalyst to carry out the fundamental application of water splitting.

Table 3. Electrochemical efficiency of Bi-based heterostructures for HER performance.

Electrochemical Systems	Fabrication Route	Current Density/mA cm^{-2}	Overpotential (η)/mV	Tafel Slope/mV dec^{-1}	Ref.
Inert 2D Bi_2O_3	Electrochemical	10	174.2	80	[25]
Bi_2S_3/Ni_3S_2/NF	Solvothermal	10	268	82	[37]
Bi_2S_3/MoS_2	Hydrothermal	10	124	123	[95]
Bi/Bi_2O_3 on Ni-foam	Hydrothermal, deposition	10	250	55	[143]
$MoSe_2$/Bi_2Se_3	Hot injection	85	300	44	[164]
$Bi_3(FeO_4)$ $(MoO_4)_2$	Solvothermal	10	207	33	[166]
Bi_2S_3@CoS_2/MoS_2	Solvothermal	10	94.7	56.2	[167]
Bi_2Se_3	Electrochemical	10	220	178	[168]
Au@Bi_2Se_3 NFs	Hot injection	10	375	78	[169]
Au@MoS_2/Bi_2S_3	Hydrothermal	10	72	40	[170]
$BiSbSe_3$NPs	Electrochemical	10	72	31.6	[171]

13. Conclusions and Perspectives

Conclusions

This review discusses the various Bismuth-based nanocatalysts used for PC, EC, and PEC applications for H_2 generation from water splitting. Bi-based nanocatalysts have gained a lot of interest due to their potential for OWS applications, having a suitable band alignment, crystal structure, optoelectronic properties, non-toxicity, cost-effectiveness, and light harvesting ability, due to which they have been discussed in this review. Electrochemical impedance (EI) and current measurements are studied for the efficiency of the nanocatalyst. However, there are certain limitations due to their poor catalytic efficiencies, back recombination, instability, lower photogenerated charge mobilization, and photo-corrosion. Thus, heterojunctions are a very promising method for reducing the recombination of photogenerated charge carriers and have been fabricated with other semiconductors to improve water splitting efficiency. This review summarizes the various Bi-based heterostructured nanocatalysts that have been exploited for PC, EC, and PEC with excellent efficiency in H_2 generation, helping to develop a nanocatalyst for enhancement of the application of H_2 generation in the future. Various Bi-based heterostructured nanocatalysts, such as TiO_2/Bi_2WO_6, Bi_2WO_6/$BiVO_4$, Bi_2O_3/Bi_2WO_6, $ZnIn_2S_4$/$BiVO_4$, Bi_2O_3/Bi_2MoO_6, Bi_2MoO_6/RGO, Bi_2WO_6/Bi_2S_3, V_2O_5/RGO/$BiVO_4$, etc., have been discussed in this review, which helps in the development of water splitting for H_2 generation. The exclusive research progress on HER performances of the heterostructured nanocatalysts is due to their enriched active sites, structural modulation, upgraded intrinsic activity, higher charge separation ability via interfacial charge transfer, and better mobility. As a result, the synergistic effect between the two or more semiconducting materials on the rate of H_2 production have been discussed in detail. Primarily, Z-scheme heterostructures are

effective catalytic systems to increase the efficiency of PC and PEC for an effective H_2 production. Ternary heterostructured nanocatalysts show higher efficiency in H_2 generation than their binary counterparts.

14. Future Perspectives

Environmentally clean and efficient energy is needed immediately to stop the usage of non-renewable energy sources. H_2 is considered a clean energy that can substitute non-renewable energy sources in the future. H_2 generation from PC, EC, and PEC is envisioned to solve the energy crisis and environmental hazards [172–178]. Although a few noteworthy achievements have been realized in Bi-based heterostructured nanocatalysts, there are still some challenges that remain, such as efficiency, applicability, and reusability as an innovative nanocatalyst for OWS. Over the past decades, there has been much research to find efficient and stable Bi-based photocatalysts for PC water splitting. Heterojunctions enhance the visible light absorption ability and charge separability, and increase the rate of H_2 generation. The challenges of Bi-based photocatalysts are thermodynamic barriers in the redox process and band alignment. Z-scheme heterostructures play a major role in increasing the efficiencies of nanocatalysts for H_2 generation. Upgradation and structural modifications are still needed in the area of PC application to make it available for industrial production. In PEC water splitting, Bismuth oxides-based heterostructured photoanodes have received much attention. Though various Bi-based catalysts are exploited for PEC applications, still they are left with a few challenges, such as cost, photo-corrosion, photostability, efficiency, etc., for the development of photoelectrodes. Experimental and theoretical strategies are important aspects for understanding the activity enhancement of the improved performance of electrocatalysts for HER and OER reactions. Bi-based heterostructures are also reviewed for EC water splitting, but in comparison to PC and PEC water splitting, there are fewer numbers of studies reported on Bi-based electrocatalysts. Electrocatalysts with high efficiency and stability need to be developed in the future with an extensive characterization for large scale applicability. The perspective of multi-functional applicability of Bi-based heterostructured catalysts towards a sustainable H_2 economy can be seen in Figure 16, which highlights the scope of these catalytic systems for scalable usage.

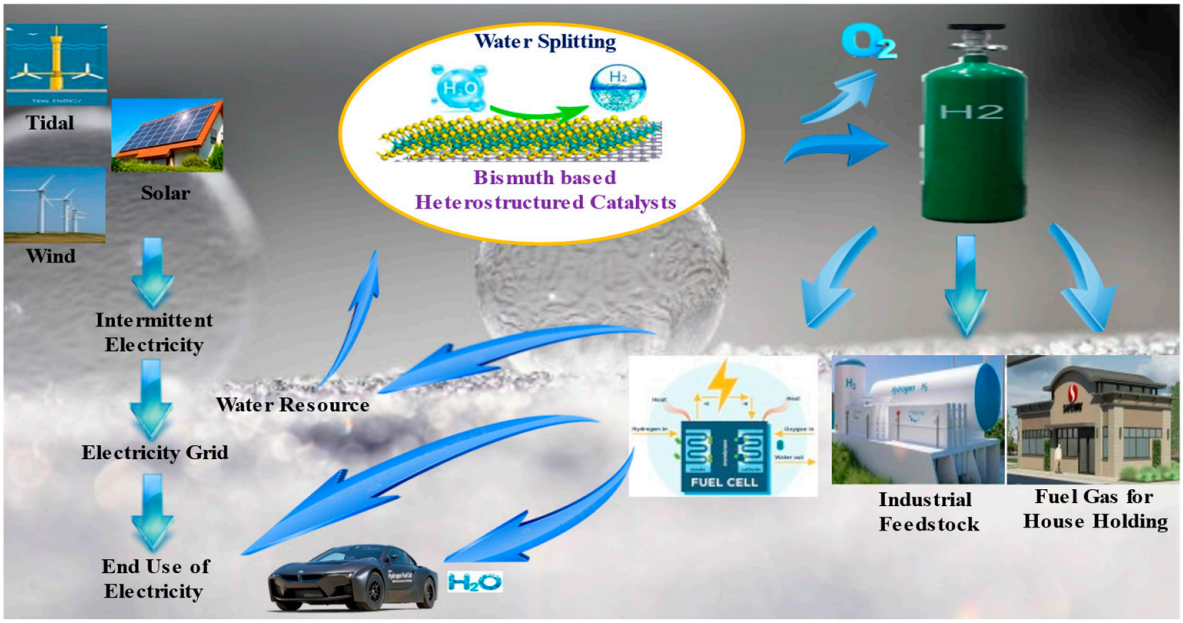


Figure 16. Schematic representation of future perspectives for hydrogen energy.

Author Contributions: S.S. is responsible for the preparation of the rough manuscript by surveying different reports and literature. I.S. collected the data and statics of the recent report. S.A.A. conducted the refinement of the manuscript. T.A. is responsible for the conceptualization, supervision, accruing funding, analysis, and finalization of the manuscript. All authors have read and agreed to the published version of the manuscript.

Funding: T.A. thanks UGC, New Delhi, Govt. of India for the Research Grant for In-service Faculty Members. The authors also Thank SERB, CSIR and MoE (SPARC/2018-2019/P843/SL) for financial support to Nano Chemistry and Nano Energy Labs.

Acknowledgments: T.A. thanks UGC, New Delhi, Govt. of India for Research Grant for In-service Faculty Members. Authors also thank SERB, CSIR and MoE (SPARC/2018-2019/P843/SL) for financial support to Nano Chemistry and Nano Energy Labs. S.S., I.S. and S.A.A. thank UGC, New Delhi for the research fellowships. Authors also acknowledge the support provided through DST PURSE program at CIF, JMI.

Conflicts of Interest: The authors declare no financial competing interest.

References

1. Lim, X. How to make the most of carbon dioxide. *Nature* **2015**, *526*, 628–631. [CrossRef] [PubMed]
2. Zhu, J.; Hu, L.; Zhao, P.; Lee, L.Y.S.; Wong, K.Y. Recent advances in electrocatalytic hydrogen evolution using nanoparticles. *Chem. Rev.* **2019**, *120*, 851–918. [CrossRef]
3. IEA. *Net Zero by 2050*; IEA: Paris, France, 2021. Available online: https://www.iea.org/reports/net-zero-by-2050 (accessed on 1 September 2022).
4. Yu, F.; Zhou, H.; Huang, Y.; Sun, J.; Qin, F.; Bao, J.; Goddard, W.A.; Chen, S.; Ren, Z. High-performance bifunctional porous non-noble metal phosphide catalyst for overall water splitting. *Nat. Commun.* **2018**, *9*, 2551. [CrossRef] [PubMed]
5. Shakya, B.D.; Aye, L.; Musgrave, P. Technical feasibility and financial analysis of hybrid wind-photovoltaic system with hydrogen storage for Cooma. *Int. J. Hydrogen Energy* **2005**, *30*, 9–20. [CrossRef]
6. Melaina, M.W.; Antonia, O.; Penev, M. *Blending Hydrogen into Natural Gas Pipeline Networks: A Review of Key Issues*; National Renewable Energy Laboratory: Washington, DC, USA, 2013.
7. Bie, C.; Wang, L.; Yu, J. Challenges for photocatalytic overall water splitting. *Chem* **2022**, *8*, 1567–1574. [CrossRef]
8. Davis, S.J.; Caldeira, K.; Matthews, H.D. Future CO_2 emissions and climate change from existing energy infrastructure. *Science* **2010**, *329*, 1330–1333. [CrossRef]
9. Dodman, D. Blaming cities for climate change? An analysis of urban greenhouse gas emissions inventories. *Environ. Urban.* **2009**, *21*, 185–201. [CrossRef]
10. Yaseen, S.; Tahir, M.B.; Wattoo, A.G. Photo-corrosion inhibition of sulphide-based nanomaterials for energy production through photocatalytic water splitting. *Int. J. Energy Res.* **2022**, *46*, 634–666. [CrossRef]
11. Chen, T.; Liu, L.; Hu, C.; Huang, H. Recent advances on Bi_2WO_6-based photocatalysts for environmental and energy applications. *Chin. J. Catal.* **2021**, *42*, 1413–1438. [CrossRef]
12. Salari, H.; Kohantorabi, M. Facile template-free synthesis of new α-MnO_2 nanorod/silver iodide p-n junction nanocomposites with high photocatalytic performance. *New J. Chem.* **2020**, *44*, 7401–7411. [CrossRef]
13. Fujishima, A.; Honda, K. Electrochemical photolysis of water at a semiconductor electrode. *Nature* **1972**, *238*, 37–38. [CrossRef] [PubMed]
14. Jain, S.K.; Farooq, U.; Jamal, F.; Kalam, A.; Ahmad, T. Hydrothermal Assisted Synthesis and Structural Characterization of Zn doped SnO_2 Nanoparticles for Catalytic Reduction of 4-Nitrophenol. *Mater. Today Proc.* **2021**, *36*, 717–723. [CrossRef]
15. Aydin, E.; Eichholtz, P.; Yönder, E. The economics of residential solar water heaters in emerging economies: The case of Turkey. *Energy Econ.* **2018**, *75*, 285–299. [CrossRef]
16. Khan, H.; Lone, I.H.; Lofland, S.E.; Ramanujachary, K.V.; Ahmad, T. Exploiting Multiferroicity of $TbFeO_3$ Nanoparticles for Hydrogen Generation through Photo/Electro/Photoelectro-catalytic Water Splitting. *Int. J. Hydrogen Energy* **2023**, *48*, 5493–5505. [CrossRef]
17. Lone, I.H.; Khan, H.; Wani, I.A.; Jain, A.K.; Ahmad, T. Magnetic, Electrical and Humidity Sensing Properties of Multiferroic $GdCrO_3$ Nanoparticles Fabricated by Metal Organic Precursor Method. *ChemistrySelect* **2022**, *7*, e202202547. [CrossRef]
18. Sadiq, I.; Ali, S.A.; Ahmad, T. Graphene-Based Derivatives Heterostructured Catalytic Systems for Sustainable Hydrogen Energy via Overall Water Splitting. *Catalysts* **2023**, *13*, 109. [CrossRef]
19. Zhang, G.; Wang, Z.; Wu, J. Construction of a Z-scheme heterojunction for high efficiency visible-light-driven photocatalytic CO_2 reduction. *Nanoscale* **2021**, *13*, 4359–4389. [CrossRef]
20. Mehtab, A.; Alshehri, S.M.; Ahmad, T. Photocatalytic and Photoelectrocatalytic Water Splitting by Porous g-C_3N_4 Nanosheets for Hydrogen Generation. *ACS Appl. Nano Mater.* **2022**, *5*, 12656–12665. [CrossRef]
21. Han, Z.; Gao, R.; Jia, Y.; Zhang, M.; Lao, Z.; Chen, B.; Zhang, Q.; Li, C.; Lv, W.; Zhou, G. Catalytic effect in Li-S batteries: From band theory to practical application. *Mater. Today* **2022**, *57*, 84–120. [CrossRef]

22. Jang, Y.J.; Lee, J.S. Photoelectrochemical water splitting with p-type metal oxide semiconductor photocathodes. *ChemSusChem* **2019**, *12*, 1835–1845. [CrossRef]
23. Odobel, F.; Le Pleux, L.; Pellegrin, Y.; Blart, E. New photovoltaic devices based on the sensitization of p-type semiconductors: Challenges and opportunities. *Acc. Chem. Res.* **2010**, *43*, 1063–1071. [CrossRef] [PubMed]
24. Meng, X.; Zhang, Z. Bismuth-based photocatalytic semiconductors: Introduction, challenges and possible approaches. *J. Mol. Catal. A Chem.* **2016**, *423*, 533–549. [CrossRef]
25. Wu, Z.; Liao, T.; Wang, S.; Mudiyanselage, J.A.; Micallef, A.S.; Li, W.; O'Mullane, A.P.; Yang, J.; Luo, W.; Ostrikov, K.; et al. Conversion of catalytically inert 2D bismuth oxide nanosheets for effective electrochemical hydrogen evolution reaction catalysis via oxygen vacancy concentration modulation. *Nano-Micro Lett.* **2022**, *14*, 90. [CrossRef]
26. Pan, B.; Wang, Y.; Liang, Y.; Luo, S.; Su, W.; Wang, X. Nanocomposite of $BiPO_4$ and reduced graphene oxide as an efficient photocatalyst for hydrogen evolution. *Int. J. Hydrogen Energy* **2014**, *39*, 13527–13533. [CrossRef]
27. Kudo, A.; Ueda, K.; Kato, H.; Mikami, I. Photocatalytic O_2 evolution under visible light irradiation on $BiVO_4$ in aqueous $AgNO_3$ solution. *Catal. Lett.* **1998**, *53*, 229–230. [CrossRef]
28. Guo, Y.; Qi, C.; Lu, B.; Li, P. Enhanced hydrogen production from water splitting by Sn-doped ZnO/BiOCl photocatalysts and Eosin Y sensitization. *Int. J. Hydrogen Energy* **2022**, *47*, 228–241. [CrossRef]
29. Zhao, J.; Yang, Y.; Yu, W.; Ma, Q.; Dong, X.; Wang, X.; Wang, J.; Liu, G. Bi_2MoO_6/RGO composite nanofibers: Facile electrospinning fabrication, structure, and significantly improved photocatalytic water splitting activity. *J. Mater. Sci. Mater. Electron.* **2017**, *28*, 543–552. [CrossRef]
30. Wu, X.; Toe, C.Y.; Su, C.; Ng, Y.H.; Amal, R.; Scott, J. Preparation of Bi-based photocatalysts in the form of powdered particles and thin films: A review. *J. Mater. Chem. A* **2020**, *8*, 15302–15318. [CrossRef]
31. Yang, H. A short review on heterojunction photocatalysts: Carrier transfer behaviour and photocatalytic mechanisms. *Mater. Res. Bull.* **2021**, *142*, 111406. [CrossRef]
32. Khan, S.U.; Al-Shahry, M.; Ingler, W.B., Jr. Efficient photochemical water splitting by a chemically modified n-TiO_2. *Science* **2002**, *297*, 2243–2245. [CrossRef]
33. Orimolade, B.O.; Idris, A.O.; Feleni, U.; Mamba, B. Recent advances in degradation of pharmaceuticals using Bi_2WO_6 mediated photocatalysis-A comprehensive review. *Environ. Pollut.* **2021**, *289*, 117891. [CrossRef] [PubMed]
34. Chachvalvutikul, A.; Luangwanta, T.; Pattisson, S.; Hutchings, G.J.; Kaowphong, S. Enhanced photocatalytic degradation of organic pollutants and hydrogen production by a visible light-responsive $Bi_2WO_6/ZnIn_2S_4$ heterojunction. *Appl. Surf. Sci.* **2021**, *544*, 148885. [CrossRef]
35. Hu, J.; Chen, C.; Zheng, Y.; Zhang, G.; Guo, C.; Li, C.M. Spatially separating redox centers on Z-scheme $ZnIn_2S_4/BiVO_4$ hierarchical heterostructure for highly efficient photocatalytic hydrogen evolution. *Small* **2020**, *16*, 2002988. [CrossRef] [PubMed]
36. Yu, H.; Jiang, H.; Wang, B.; Huang, X.; Yuan, J.; Huang, J.; Zhang, J.; Zeng, G. Modulation of Bi_2MoO_6-based materials for photocatalytic water splitting and environmental application: A critical review. *Small* **2019**, *15*, 1901008. [CrossRef] [PubMed]
37. Wang, S.; Xue, W.; Fang, Y.; Li, Y.; Yan, L.; Wang, W.; Zhao, R. Bismuth activated succulent-like binary metal sulfide heterostructure as a binder-free electrocatalyst for enhanced oxygen evolution reaction. *J. Colloid Interface Sci.* **2020**, *573*, 150–157. [CrossRef] [PubMed]
38. Baek, J.H.; Kim, B.J.; Han, G.S.; Hwang, S.W.; Kim, D.R.; Cho, I.S.; Jung, H.S. $BiVO_4/WO_3/SnO_2$ double-heterojunction photoanode with enhanced charge separation and visible-transparency for bias-free solar water-splitting with a perovskite solar cell. *ACS Appl. Mater. Interfaces* **2017**, *9*, 1479–1487. [CrossRef]
39. Kallawar, G.A.; Barai, D.P.; Bhanvase, B.A. Bismuth titanate based photocatalysts for degradation of persistent organic compounds in wastewater: A comprehensive review on synthesis methods, performance as photocatalyst and challenges. *J. Clean. Prod.* **2021**, *318*, 128563. [CrossRef]
40. Theerthagiri, J.; Chandrasekaran, S.; Salla, S.; Elakkiya, V.; Senthil, R.A.; Nithyadharseni, P.; Maiyalagan, T.; Micheal, K.; Ayeshamariam, A.; Arasu, M.V. Recent developments of metal oxide based heterostructures for photocatalytic applications towards environmental remediation. *J. Solid State Chem.* **2018**, *267*, 35–52. [CrossRef]
41. Zhang, N.; Ciriminna, R.; Pagliaro, M.; Xu, Y.J. Nanochemistry-derived Bi_2WO_6 nanostructures: Towards production of sustainable chemicals and fuels induced by visible light. *Chem. Soc. Rev.* **2014**, *43*, 5276–5287. [CrossRef]
42. Hassan, J.Z.; Raza, A.; Qumar, U.; Li, G. Recent advances in engineering strategies of Bi-based photocatalysts for environmental remediation. *Sustain. Mater. Technol.* **2022**, e00478. [CrossRef]
43. Weon, S.; He, F.; Choi, W. Status and challenges in photocatalytic nanotechnology for cleaning air polluted with volatile organic compounds: Visible light utilization and catalyst deactivation. *Environ. Sci. Nano* **2019**, *6*, 3185–3214. [CrossRef]
44. Han, N.; Ding, P.; He, L.; Li, Y.; Li, Y. Promises of main group metal–based nanostructured materials for electrochemical CO_2 reduction to formate. *Adv. Energy Mater.* **2020**, *10*, 1902338. [CrossRef]
45. Wei, Z.; Liu, J.; Shangguan, W. A review on photocatalysis in antibiotic wastewater: Pollutant degradation and hydrogen production. *Chin. J. Catal.* **2020**, *41*, 1440–1450. [CrossRef]
46. An, X.; Li, S.; Hao, X.; Xie, Z.; Du, X.; Wang, Z.; Hao, X.; Abudula, A.; Guan, G. Common strategies for improving the performances of tin and bismuth-based catalysts in the electrocatalytic reduction of CO_2 to formic acid/formate. *Renew. Sustain. Energ. Rev.* **2021**, *143*, 110952. [CrossRef]

47. Kim, J.H.; Jang, J.W.; Jo, Y.H.; Abdi, F.F.; Lee, Y.H.; Krol, R.V.D.; Lee, J.S. Hetero-type dual photoanodes for unbiased solar water splitting with extended light harvesting. *Nat. Commun.* **2016**, *7*, 13380. [CrossRef]
48. Wu, Z.; Liu, J.; Tian, Q.; Wu, W. Efficient Visible Light Formaldehyde Oxidation with 2D p-n Heterostructure of BiOBr/$BiPO_4$ Nanosheets at Room Temperature. *ACS Sustain. Chem. Eng.* **2017**, *5*, 5008–5017. [CrossRef]
49. Zhang, X.; Wang, Y.; Liu, B.; Sang, Y.; Liu, H. Heterostructures construction on TiO_2 nanobelts: A powerful tool for building high-performance photocatalysts. *Appl. Catal. B* **2017**, *202*, 620–641. [CrossRef]
50. Wang, M.; Han, J.; Hu, Y.; Guo, R.; Yin, Y. Carbon-incorporated NiO/TiO_2 mesoporous shells with p-n heterojunctions for efficient visible light photocatalysis. *ACS Appl. Mater. Interfaces* **2016**, *8*, 29511–29521. [CrossRef]
51. Li, Y.; Zhang, J.Z. Hydrogen generation from photoelectrochemical water splitting based on nanomaterials. *Laser Photonics Rev.* **2010**, *4*, 517–528. [CrossRef]
52. Di, T.; Xu, Q.; Ho, W.; Tang, H.; Xiang, Q.; Yu, J. Review on metal sulphide-based Z-scheme photocatalysts. *ChemCatChem* **2019**, *11*, 1394–1411. [CrossRef]
53. Yaw, C.S.; Ruan, Q.; Tang, J.; Soh, A.K.; Chong, M.N. A Type II n-n staggered orthorhombic V_2O_5/monoclinic clinobisvanite $BiVO_4$ heterojunction photoanode for photoelectrochemical water oxidation: Fabrication, characterisation and experimental validation. *Chem. Eng. J.* **2019**, *364*, 177–185. [CrossRef]
54. Cheng, B.Y.; Yang, J.S.; Cho, H.W.; Wu, J.J. Fabrication of an efficient $BiVO_4$-TiO_2 heterojunction photoanode for photoelectrochemical water oxidation. *ACS Appl. Mater. Interfaces* **2016**, *8*, 20032–20039. [CrossRef] [PubMed]
55. Wetchakun, N.; Chaiwichain, S.; Inceesungvorn, B.; Pingmuang, K.; Phanichphant, S.; Minett, A.I.; Chen, J. $BiVO_4$/CeO_2 nanocomposites with high visible-light-induced photocatalytic activity. *ACS Appl. Mater. Interfaces* **2012**, *4*, 3718–3723. [CrossRef] [PubMed]
56. Xu, Q.; Zhang, L.; Cheng, B.; Fan, J.; Yu, J. S-scheme heterojunction photocatalyst. *Chem* **2020**, *6*, 1543–1559. [CrossRef]
57. Tada, H.; Mitsui, T.; Kiyonaga, T.; Akita, T.; Tanaka, K. All-solid-state Z-scheme in CdS-Au-TiO_2 three-component nanojunction system. *Nat. Mater.* **2006**, *5*, 782–786. [CrossRef]
58. Kudo, A.; Kato, H.; Tsuji, I. Strategies for the development of visible-light-driven photocatalysts for water splitting. *Chem. Lett.* **2004**, *33*, 1534–1539. [CrossRef]
59. Dai, X.J.; Luo, Y.S.; Zhang, W.D.; Fu, S.Y. Facile hydrothermal synthesis and photocatalytic activity of bismuth tungstate hierarchical hollow spheres with an ultrahigh surface area. *Dalton Trans.* **2010**, *39*, 3426–3432. [CrossRef]
60. Zhang, L.; Bahnemann, D. Synthesis of nanovoid Bi_2WO_6 2D ordered arrays as photoanodes for photoelectrochemical water splitting. *ChemSusChem.* **2013**, *6*, 283–290. [CrossRef]
61. Dutta, V.; Sharma, S.; Raizada, P.; Hosseini-Bandegharaei, A.; Kaushal, J.; Singh, P. Fabrication of visible light active $BiFeO_3$/CuS/SiO_2 Z-scheme photocatalyst for efficient dye degradation. *Mater. Lett.* **2020**, *270*, 127693. [CrossRef]
62. Wan, S.; Ou, M.; Zhong, Q.; Zhang, S.; Song, F. Construction of Z-scheme photocatalytic systems using $ZnIn_2S_4$, CoOx-loaded Bi_2MoO_6 and reduced graphene oxide electron mediator and its efficient non sacrificial water splitting under visible light. *Chem. Eng. J.* **2017**, *325*, 690–699. [CrossRef]
63. Dai, G.; Yu, J.; Liu, G. Synthesis and enhanced visible-light photoelectrocatalytic activity of p-n junction BiOI/TiO_2 nanotube arrays. *J. Phys. Chem. C* **2011**, *115*, 7339–7346. [CrossRef]
64. Liu, Y.; He, J.; Qi, Y.; Wang, Y.; Long, F.; Wang, M. Preparation of flower-like BiOBr/Bi_2WO_6 Z-scheme heterojunction through an ion exchange process with enhanced photocatalytic activity. *Mater. Sci. Semicond. Process.* **2022**, *137*, 106195. [CrossRef]
65. Feng, C.; Wang, D.; Jin, B.; Jiao, Z. The enhanced photocatalytic properties of BiOCl/$BiVO_4$ p-n heterojunctions via plasmon resonance of metal Bi. *RSC Adv.* **2015**, *5*, 75947–75952. [CrossRef]
66. Zhang, J.; Liu, H.; Ma, Z. Flower-like Ag_2O/Bi_2MoO_6 p-n heterojunction with enhanced photocatalytic activity under visible light irradiation. *J. Mol. Catal. A Chem.* **2016**, *424*, 37–44. [CrossRef]
67. Hasija, V.; Kumar, A.; Sudhaik, A.; Raizada, P.; Singh, P.; Van Le, Q.; Le, T.T.; Nguyen, V.H. Step-scheme heterojunction photocatalysts for solar energy, water splitting, CO_2 conversion, and bacterial inactivation: A review. *Environ. Chem. Lett.* **2021**, *19*, 2941–2966. [CrossRef]
68. Lu, H.; Hao, Q.; Chen, T.; Zhang, L.; Chen, D.; Ma, C.; Yao, W.; Zhu, Y. A high-performance Bi_2O_3/Bi_2SiO_5 p-n heterojunction photocatalyst induced by phase transition of Bi_2O_3. *Appl. Catal. B* **2018**, *237*, 59–67. [CrossRef]
69. Peng, Y.; Yan, M.; Chen, Q.G.; Fan, C.M.; Zhou, H.Y.; Xu, A.W. Novel one-dimensional Bi_2O_3-Bi_2WO_6 p-n hierarchical heterojunction with enhanced photocatalytic activity. *J. Mater. Chem. A* **2014**, *2*, 8517–8524. [CrossRef]
70. Arunkumar, M.; Veerakumar, S.; Mohanavel, V.; Vairamuthu, J.; Vijayan, V.; Senthilkumar, N. A Novel Visible Light-Driven p-Type $BiFeO_3$/n-Type SnS2 Heterojunction Photocatalyst for Efficient Charge Separation and Enhanced Photocatalytic Activity. *J. Clust. Sci.* **2021**, *32*, 1431–1439. [CrossRef]
71. Chen, C.; Cai, W.; Long, M.; Zhou, B.; Wu, Y.; Wu, D.; Feng, Y. Synthesis of visible-light responsive graphene oxide/TiO_2 composites with p-n heterojunction. *ACS Nano* **2010**, *4*, 6425–6432. [CrossRef]
72. Luo, B.; Xu, D.; Li, D.; Wu, G.; Wu, M.; Shi, W.; Chen, M. Fabrication of an Ag/Bi_3TaO_7 plasmonic photocatalyst with enhanced photocatalytic activity for degradation of tetracycline. *ACS Appl. Mater. Interfaces* **2015**, *7*, 17061–17069. [CrossRef]
73. Zhang, C.; Zhu, Y. Synthesis of square Bi_2WO_6 nanoplates as high-activity visible-light-driven photocatalysts. *Chem. Mater.* **2005**, *17*, 3537–3545. [CrossRef]

74. Sharma, S.; Kumar, D.; Khare, N. Plasmonic Ag nanoparticles decorated Bi_2S_3 nanorods and nanoflowers: Their comparative assessment for photoelectrochemical water splitting. *Int. J. Hydrogen Energy* **2019**, *44*, 3538–3552. [CrossRef]
75. Muruganandham, M.; Suri, R.P.; Sillanpää, M.; Wu, J.J.; Ahmmad, B.; Balachandran, S.; Swaminathan, M. Recent developments in heterogeneous catalyzed environmental remediation processes. *J. Nanosci. Nanotechnol.* **2014**, *14*, 1898–1910. [CrossRef] [PubMed]
76. Chen, Z.; Jiang, X.; Zhu, C.; Shi, C. Chromium-modified $Bi_4Ti_3O_{12}$ photocatalyst: Application for hydrogen evolution and pollutant degradation. *Appl. Catal. B* **2016**, *199*, 241–251. [CrossRef]
77. Jain, S.K.; Fazil, M.; Naaz, F.; Pandit, N.A.; Ahmed, J.; Alshehri, S.M.; Mao, Y.; Ahmad, T. Silver-doped SnO_2 nanostructures for photocatalytic water splitting and catalytic nitrophenol reduction. *New J. Chem.* **2022**, *46*, 2846–2857. [CrossRef]
78. Fu, Y.; Zhao, J.; Wang, H.; Huang, H.; Liu, Y.; Dou, Y.; Shao, M.; Kang, Z. All-solid-state Z-scheme system of NiO/CDs/$BiVO_4$ for visible light-driven efficient overall water splitting. *Chem. Eng. J.* **2019**, *358*, 134–142.
79. Jain, S.K.; Fazil, M.; Pandit, N.A.; Ali, S.A.; Naaz, F.; Khan, H.; Mehtab, A.; Ahmed, J.; Ahmad, T. Modified, Solvothermally Derived Cr-doped SnO_2 Nanostructures for Enhanced Photocatalytic and Electrochemical Water-Splitting Applications. *ACS Omega* **2022**, *7*, 14138–14147. [CrossRef]
80. Lone, I.H.; Khan, H.; Jain, A.K.; Ahmed, J.; Ramanujachary, K.V.; Ahmad, T. Metal Organic Precursor Synthesis, Structural Characterization and Multiferroic Properties of $GdFeO_3$ Nanoparticles. *ACS Omega* **2022**, *7*, 33908–33915. [CrossRef]
81. Ahmad, T.; Ganguli, A.K. Structural and dielectric characterization of nanocrystalline (Ba, Pb)ZrO_3 developed by reverse micellar synthesis. *J. Am. Ceram. Soc.* **2006**, *89*, 3140–3146. [CrossRef]
82. Song, Y.; Zou, W.; Lu, Q.; Lin, L.; Liu, Z. Graphene transfer: Paving the road for applications of chemical vapor deposition graphene. *Small* **2021**, *17*, 2007600. [CrossRef]
83. Samsudin, M.F.R.; Sufian, S.; Mohamed, N.M.; Bashiri, R.; Wolfe, F.; Ramli, R.M. Enhancement of hydrogen production over screen-printed TiO_2/$BiVO_4$ thin film in the photoelectrochemical cells. *Mater. Lett.* **2018**, *211*, 13–16. [CrossRef]
84. Hu, Y.; Jia, Z.; Lv, R.; Fan, C.; Zhang, H. One-pot electrochemical preparation of BiOCl/$BiPO_4$ double-layer heterojunction film with efficient photocatalytic performance. *Mater. Res. Bull.* **2017**, *94*, 222–230. [CrossRef]
85. Li, Z.; Tian, Y. Nano-Bismuth-Sulfide for Advanced Optoelectronics. *Photonics* **2022**, *9*, 790. [CrossRef]
86. Li, W.; Yang, J.; Jiang, Q.; Luo, Y.; Hou, Y.; Zhou, S.; Xiao, Y.; Fu, L.; Zhou, Z. Electrochemical atomic layer deposition of Bi_2S_3/Sb_2S_3 quantum dots co-sensitized TiO_2 nanorods solar cells. *J. Power Sources* **2016**, *307*, 690–696. [CrossRef]
87. Chai, W.; Yang, F.; Yin, W.; You, S.; Wang, K.; Ye, W.; Rui, Y.; Tang, B. Bi_2S_3/C nanorods as efficient anode materials for lithium-ion batteries. *Dalton Trans.* **2019**, *48*, 1906–1914. [CrossRef]
88. Chao, J.; Xing, S.; Liu, Z.; Zhang, X.; Zhao, Y.; Zhao, L.; Fan, Q. Large-scale synthesis of Bi_2S_3 nanorods and nanoflowers for flexible near-infrared laser detectors and visible light photodetectors. *Mater. Res. Bull.* **2018**, *98*, 194–199. [CrossRef]
89. Ajiboye, T.O.; Onwudiwe, D.C. Bismuth sulfide-based compounds: Properties, synthesis and applications. *Results Chem.* **2021**, *3*, 100151. [CrossRef]
90. Cheng, Y.; Chang, Y.; Feng, Y.; Jian, H.; Wu, X.; Zheng, R.; Xu, K.; Zhang, H. Bismuth sulfide nanorods with retractable zinc protoporphyrin molecules for suppressing innate antioxidant defense system and strengthening phototherapeutic effects. *Adv. Mater.* **2019**, *31*, 1806808. [CrossRef]
91. Cui, Y.; Li, M.; Zhu, N.; Cheng, Y.; Lam, S.S.; Chen, J.; Gao, Y.; Zhao, J. Bi-based visible light-driven nano-photocatalyst: The design, synthesis, and its application in pollutant governance and energy development. *Nano Today* **2022**, *43*, 101432. [CrossRef]
92. Xu, M.; Yang, J.; Sun, C.; Liu, L.; Cui, Y.; Liang, B. Performance enhancement strategies of bi-based photocatalysts: A review on recent progress. *Chem. Eng. J.* **2020**, *389*, 124402. [CrossRef]
93. Xu, D.; Liu, Y.; Liu, Y.; Chen, F.; Zhang, C.; Liu, B. A review on recent progress in the development of photoelectrodes for photocathodic protection: Design, properties, and prospects. *Mater. Des.* **2021**, *197*, 109235. [CrossRef]
94. Mahadik, M.A.; Chung, H.S.; Lee, S.Y.; Cho, M.; Jang, J.S. In-situ noble fabrication of Bi_2S_3/$BiVO_4$ hybrid nanostructure through a photoelectrochemical transformation process for solar hydrogen production. *ACS Sustain. Chem. Eng.* **2018**, *6*, 12489–12501. [CrossRef]
95. Zhou, L.; Yang, T.; Chen, S.; Gao, J.; Wang, X.; He, P.; Lei, H.; Yang, D.; Dong, F.; Jia, L.; et al. Tunably fabricated nanotremella-like Bi_2S_3/MoS_2: An excellent and highly stable electrocatalyst for alkaline hydrogen evolution reaction. *Int. J. Hydrogen Energy* **2020**, *45*, 9535–9545. [CrossRef]
96. Hao, L.X.; Chen, G.; Yu, Y.G.; Zhou, Y.S.; Han, Z.H.; Liu, Y. Sonochemistry synthesis of Bi_2S_3/CdS heterostructure with enhanced performance for photocatalytic hydrogen evolution. *Int. J. Hydrogen Energy* **2014**, *39*, 14479–14486. [CrossRef]
97. Ahmad, A.; Tezcan, F.; Yerlikaya, G.; Paksoy, H.; Kardaş, G. Three-dimensional rosette-rod TiO_2/Bi_2S_3 heterojunction for enhanced photoelectrochemical water splitting. *J. Alloys Compd.* **2021**, *868*, 159133. [CrossRef]
98. Sadhasivam, S.; Anbarasan, N.; Mukilan, M.; Manivel, P.; Jeganathan, K. Bi_2S_3 anchored ZnS/ZnO nanorod arrays photoanode for enhanced visible light driven photo electrochemical properties. *Int. J. Hydrogen Energy* **2020**, *45*, 30080–30090. [CrossRef]
99. Wei, J.; Zhou, C.; Xin, Y.; Li, X.; Zhao, L.; Liu, Z. Cooperation effect of heterojunction and co-catalyst in $BiVO_4$/Bi_2S_3/NiOOH photoanode for improving photoelectrochemical performances. *New J. Chem.* **2018**, *42*, 19415–19422. [CrossRef]
100. Wang, Y.; Tian, W.; Chen, L.; Cao, F.; Guo, J.; Li, L. Three-dimensional WO_3 nanoplate/Bi_2S_3 nanorod heterojunction as a highly efficient photoanode for improved photoelectrochemical water splitting. *ACS Appl. Mater. Interfaces* **2017**, *9*, 40235–40243. [CrossRef]

101. Subramanyam, P.; Meena, B.; Neeraja Sinha, G.; Suryakala, D.; Subrahmanyam, C. Facile synthesis and photoelectrochemical performance of a Bi_2S_3@ rGO nanocomposite photoanode for efficient water splitting. *Energy Fuels* **2021**, *35*, 6315–6321. [CrossRef]
102. Zhu, Z.; Wan, S.; Zhao, Y.; Qin, Y.; Ge, X.; Zhong, Q.; Bu, Y. Recent progress in Bi_2WO_6-based photocatalysts for clean energy and environmental remediation: Competitiveness, challenges, and future perspectives. *Nano Select* **2021**, *2*, 187–215. [CrossRef]
103. Li, C.; Chen, G.; Sun, J.; Feng, Y.; Liu, J.; Dong, H. Ultrathin nanoflakes constructed erythrocyte-like Bi_2WO_6 hierarchical architecture via anionic self-regulation strategy for improving photocatalytic activity and gas-sensing property. *Appl. Catal. B* **2015**, *163*, 415–423. [CrossRef]
104. Zhao, G.; Hao, S.; Xing, Y.; Wang, Y.; Wang, Y.; Xu, K.; Xu, X. Preparation of Low-Dimensional Bismuth Tungstate (Bi_2WO_6) Photocatalyst by Electrospinning. *Phys. Status Solidi* **2019**, *216*, 1900035. [CrossRef]
105. Yi, H.; Qin, L.; Huang, D.; Zeng, G.; Lai, C.; Liu, X.; Li, B.; Wang, H.; Zhou, C.; Huang, F.; et al. Nano-structured bismuth tungstate with controlled morphology: Fabrication, modification, environmental application and mechanism insight. *Chem. Eng. J.* **2019**, *358*, 480–496. [CrossRef]
106. Wu, S.; Sun, J.; Li, Q.; Hood, Z.D.; Yang, S.; Su, T.; Peng, R.; Wu, Z.; Sun, W.; Kent, P.R.; et al. Effects of surface terminations of 2D Bi_2WO_6 on photocatalytic hydrogen evolution from water splitting. *ACS Appl. Mater. Interfaces* **2020**, *12*, 20067–20074. [CrossRef] [PubMed]
107. Chao, P.Y.; Chang, C.J.; Lin, K.S.; Wang, C.F. Synergistic effects of morphology control and calcination on the activity of flower-like Bi_2WO_6-Bi_2O_3 photocatalysts prepared by an ionic liquid-assisted solvothermal method. *J. Alloys Compd.* **2021**, *883*, 160920. [CrossRef]
108. Hu, H.; Kong, W.; Wang, J.; Liu, C.; Cai, Q.; Kong, Y.; Zhou, S.; Yang, Z. Engineering 2D compressed layered g-C3N4 nanosheets by the intercalation of $BiVO_4$-Bi_2WO_6 composites for boosting photocatalytic activities. *Appl. Surf. Sci.* **2021**, *557*, 149796. [CrossRef]
109. Parnicka, P.; Mikolajczyk, A.; Pinto, H.P.; Lisowski, W.; Klimczuk, T.; Trykowski, G.; Bajorowicz, B.; Zaleska-Medynska, A. Experimental and DFT insights into an eco-friendly photocatalytic system toward environmental remediation and hydrogen generation based on $AgInS_2$ quantum dots embedded on Bi_2WO_6. *Appl. Surf. Sci.* **2020**, *525*, 146596. [CrossRef]
110. Sun, F.; Qi, H.; Xie, Y. Flexible self-supporting bifunctional [TiO_2/C]//[Bi_2WO_6/C] carbon-based Janus nanofiber heterojunction photocatalysts for efficient hydrogen evolution and degradation of organic pollutant. *J. Alloys Compd.* **2020**, *830*, 154673. [CrossRef]
111. Xiong, S.; Bao, S.; Wang, W.; Hao, J.; Mao, Y.; Liu, P.; Huang, Y.; Duan, Z.; Lv, Y.; Ouyang, D. Surface oxygen vacancy and graphene quantum dots co-modified Bi_2WO_6 toward highly efficient photocatalytic reduction of CO_2. *Appl. Catal. B* **2022**, *305*, 121026. [CrossRef]
112. Fazil, M.; Ahmad, T. Pristine TiO_2 and Sr-Doped TiO_2 Nanostructures for Enhanced Photocatalytic and Electrocatalytic Water Splitting Applications. *Catalysts* **2023**, *13*, 93. [CrossRef]
113. Xiong, J.; Song, P.; Di, J.; Li, H.; Liu, Z. Freestanding ultrathin bismuth-based materials for diversified photocatalytic applications. *J. Mater. Chem. A* **2019**, *7*, 25203–25226. [CrossRef]
114. Shi, F.; Huang, K.; Feng, S. Recent advances on black phosphorus based electrocatalysts for water-splitting. *ChemCatChem* **2020**, *12*, 1913–1921. [CrossRef]
115. Sun, Z.; Guo, J.; Zhu, S.; Mao, L.; Ma, J.; Zhang, D. A high-performance Bi_2WO_6 -graphene photocatalyst for visible light-induced H_2 and O_2 generation. *Nanoscale* **2014**, *6*, 2186–2193. [CrossRef] [PubMed]
116. Zhou, Y.; Zhang, Y.; Lin, M.; Long, J.; Zhang, Z.; Lin, H.; Wu, J.C.S.; Wang, X. Monolayered Bi_2WO_6 nanosheets mimicking heterojunction interface with open surfaces for photocatalysis. *Nat. Commun.* **2015**, *6*, 8340. [CrossRef]
117. Nasir, J.A.; Munir, A.; Ahmad, N.; Haq, T.U.; Khan, Z.; Rehman, Z. Photocatalytic Z-Scheme Overall Water Splitting: Recent Advances in Theory and Experiments. *Adv. Mater.* **2021**, *33*, 2105195. [CrossRef]
118. Zhao, J.; Yang, Y.; Dong, X.; Ma, Q.; Yu, W.; Wang, J.; Liu, G. Electrospinning construction of Bi_2WO_6/RGO composite nanofibers with significantly enhanced photocatalytic water splitting activity. *RSC Adv.* **2016**, *6*, 64741–64748. [CrossRef]
119. Arif, M.; Min, Z.; Yuting, L.; Yin, H.; Liu, X. A Bi_2WO_6-based hybrid heterostructures photocatalyst with enhanced photodecomposition and photocatalytic hydrogen evolution through Z-scheme process. *J. Ind. Eng. Chem.* **2019**, *69*, 345–357. [CrossRef]
120. Joy, J.; Mathew, J.; George, S.C. Nanomaterials for photoelectrochemical water splitting—Review. *Int. J. Hydrogen Energy* **2018**, *43*, 4804–4817. [CrossRef]
121. Dabodiya, T.S.; Selvarasu, P.; Murugan, A.V. Tetragonal to monoclinic crystalline phases change of $BiVO_4$ via microwave-hydrothermal reaction: In correlation with visible-light-driven photocatalytic performance. *Inorg. Chem.* **2019**, *58*, 5096–5110. [CrossRef]
122. Ikram, A.; Zulfequar, M.; Satsangi, V.R. Role and prospects of green quantum dots in photoelectrochemical hydrogen generation: A review. *Int. J. Hydrogen Energy* **2022**, *47*, 11472–11491. [CrossRef]
123. Xia, L.; Bai, J.; Li, J.; Zeng, Q.; Li, L.; Zhou, B. High-performance $BiVO_4$ photoanodes cocatalyzed with an ultrathin α-Fe_2O_3 layer for photoelectrochemical application. *Appl. Catal. B* **2017**, *204*, 127–133. [CrossRef]
124. Zhu, M.; Sun, Z.; Fujitsuka, M.; Majima, T. Z-scheme photocatalytic water splitting on a 2D heterostructure of black phosphorus/bismuth vanadate using visible light. *Angew. Chem. Int. Ed.* **2018**, *57*, 2160–2164. [CrossRef]
125. Sitaaraman, S.R.; Shanmugapriyan, M.I.; Varunkumar, K.; Grace, A.N.; Sellappan, R. Synthesis of heterojunction tungsten oxide (WO_3) and Bismuth vanadate ($BiVO_4$) photoanodes by spin coating method for solar water splitting applications. *Mater. Today Proc.* **2021**, *45*, 3920–3926. [CrossRef]

126. Di Valentin, C.; Pacchioni, G. Spectroscopic properties of doped and defective semiconducting oxides from hybrid density functional calculations. *Acc. Chem. Res.* **2014**, *47*, 3233–3241. [CrossRef] [PubMed]
127. Kalanoor, B.S.; Seo, H.; Kalanur, S.S. Recent developments in photoelectrochemical water-splitting using WO_3/$BiVO_4$ heterojunction photoanode: A review. *Mater. Sci. Technol.* **2018**, *1*, 49–62.
128. Yaw, C.S.; Ng, W.C.; Ruan, Q.; Tang, J.; Soh, A.K.; Chong, M.N. Tuning of reduced graphene oxide thin film as an efficient electron conductive interlayer in a proven heterojunction photoanode for solar-driven photoelectrochemical water splitting. *J. Alloys Compd.* **2020**, *817*, 152721. [CrossRef]
129. Majumder, S.; Gu, M.; Kim, K.H. Facile fabrication of $BiVO_4$/Bi_2S_3/$NiCoO_2$ for significant photoelectrochemical water splitting. *Appl. Surf. Sci.* **2022**, *574*, 151562. [CrossRef]
130. Fang, G.; Liu, Z.; Han, C.; Ma, X.; Lv, H.; Huang, C.; Cheng, Z.; Tong, Z.; Wang, P. $CoNiO_2$ as a novel water oxidation cocatalyst to enhance PEC water splitting performance of $BiVO_4$. *Soc. Chem.* **2020**, *64*, 9158–9161.
131. Dou, L.; Jin, X.; Chen, J.; Zhong, J.; Li, J.; Zeng, Y.; Duan, R. One-pot solvothermal fabrication of S-scheme OVs-Bi_2O_3/Bi_2SiO_5 microsphere heterojunctions with enhanced photocatalytic performance toward decontamination of organic pollutants. *Appl. Surf. Sci.* **2020**, *527*, 146775. [CrossRef]
132. Fu, F.; Shen, H.; Xue, W.; Zhen, Y.; Soomro, R.A.; Yang, X.; Wang, D.; Xu, B.; Chi, R. Alkali-assisted synthesis of direct Z-scheme based Bi_2O_3/Bi_2MoO_6 photocatalyst for highly efficient photocatalytic degradation of phenol and hydrogen evolution reaction. *J. Catal.* **2019**, *375*, 399–409. [CrossRef]
133. Shafiq, F.; Tahir, M.B.; Hussain, A.; Sagir, M.; ur Rehman, J.; Kebaili, I.; Alrobei, H.; Alzaid, M. The construction of a highly efficient p-n heterojunction Bi_2O_3/$BiVO_4$ for hydrogen evolution through solar water splitting. *Int. J. Hydrogen Energy* **2022**, *47*, 4594–4600. [CrossRef]
134. Goud, B.S.; Koyyada, G.; Jung, J.H.; Reddy, G.R.; Shim, J.; Nam, N.D.; Vattikuti, S.V.P. Surface oxygen vacancy facilitated Z-scheme MoS_2/Bi_2O_3 heterojunction for enhanced visible-light driven photocatalysis-pollutant degradation and hydrogen production. *Int. J. Hydrogen Energy* **2020**, *45*, 18961–18975. [CrossRef]
135. Ali, S.A.; Ahmad, T. Chemical strategies in molybdenum-based chalcogenides nanostructures for photocatalysis. *Int. J. Hydrogen Energy* **2022**, *47*, 29255–29283. [CrossRef]
136. Ye, L.; Deng, Y.; Wang, L.; Xie, H.; Su, F. Bismuth-based photocatalysts for solar photocatalytic carbon dioxide conversion. *ChemSusChem* **2019**, *12*, 3671–3701. [CrossRef] [PubMed]
137. Mohapatra, L.; Parida, K. A review on the recent progress, challenges and perspective of layered double hydroxides as promising photocatalysts. *J. Mater. Chem. A* **2016**, *4*, 10744–10766. [CrossRef]
138. Yang, X.; Xu, X.; Wang, J.; Chen, T.; Wang, S.; Ding, X.; Chen, H. Insights into the surface/interface modifications of Bi_2MoO_6: Feasible strategies and photocatalytic applications. *Sol. RRL* **2021**, *5*, 2000442. [CrossRef]
139. Stelo, F.; Kublik, N.; Ullah, S.; Wender, H. Recent advances in Bi_2MoO_6 based Z-scheme heterojunctions for photocatalytic degradation of pollutants. *J. Alloys Compd.* **2020**, *829*, 154591. [CrossRef]
140. Zhao, H.; Tian, F.; Wang, R.; Chen, R. A review on bismuth-related nanomaterials for photocatalysis. *Rev. Adv. Mater. Sci.* **2014**, *3*, 3–27. [CrossRef]
141. Ye, K.H.; Yu, X.; Qiu, Z.; Zhu, Y.; Lu, X.; Zhang, Y. Facile synthesis of bismuth oxide/bismuth vanadate heterostructures for efficient photoelectrochemical cells. *RSC Adv.* **2015**, *5*, 34152–34156. [CrossRef]
142. SalomŃo, P.E.A.; de Souza Barbosa, L.R.; Andrade, T.S.; da Cruz Ferreira, E.J.; Pereira, M.C. $ZnBi_{38}O_{60}$/Bi_2O_3 photocathode for hydrogen production from water splitting. *Int. J. Hydrogen Energy* **2019**, *44*, 28603–28612. [CrossRef]
143. Syah, R.; Ahmad, A.; Davarpanah, A.; Elveny, M.; Ramdan, D.; Albaqami, M.D.; Ouladsmane, M. Incorporation of Bi_2O_3 residuals with metallic bi as high performance electrocatalyst toward hydrogen evolution reaction. *Catalysts* **2021**, *11*, 1099. [CrossRef]
144. Salomão, P.E.; Gomes, D.S.; Ferreira, E.J.; Moura, F.; Nascimento, L.L.; Patrocínio, A.O.; Pereira, M.C. Photoelectrochemical hydrogen production from water splitting using heterostructured nanowire arrays of Bi_2O_3/BiAl oxides as a photocathode. *Sol. Energy Mater Sol. Cells* **2019**, *194*, 276–284. [CrossRef]
145. Walter, M.G.; Warren, E.L.; McKone, J.R.; Boettcher, S.W.; Mi, Q.; Santori, E.A.; Lewis, N.S. Solar water splitting cells. *Chem. Rev.* **2010**, *110*, 6446–6473. [CrossRef] [PubMed]
146. Fajrina, N.; Tahir, M. A critical review in strategies to improve photocatalytic water splitting towards hydrogen production. *Int. J. Hydrogen Energy* **2019**, *44*, 540–577. [CrossRef]
147. Li, J.; Yin, Y.; Liu, E.; Ma, Y.; Wan, J.; Fan, J.; Hu, X. In situ growing Bi_2MoO_6 on g-C3N4 nanosheets with enhanced photocatalytic hydrogen evolution and disinfection of bacteria under visible light irradiation. *J. Hazard. Mater.* **2017**, *321*, 183–192. [CrossRef]
148. Mei, F.; Zhang, J.; Dai, K.; Zhu, G.; Liang, C. A Z-scheme Bi_2MoO_6/CdSe-diethylenetriamine heterojunction for enhancing photocatalytic hydrogen production activity under visible light. *Dalton Trans.* **2019**, *48*, 1067–1074. [CrossRef]
149. Zhao, Y.; Fan, H.; Fu, K.; Ma, L.; Li, M.; Fang, J. Intrinsic electric field assisted polymeric graphitic carbon nitride coupled with $Bi_4Ti_3O_{12}$/$Bi_2Ti_2O_7$ heterostructure nanofibers toward enhanced photocatalytic hydrogen evolution. *Int. J. Hydrogen Energy* **2016**, *41*, 16913–16926. [CrossRef]
150. Bae, S.Y.; Mahmood, J.; Jeon, I.Y.; Baek, J.B. Recent advances in ruthenium-based electrocatalysts for the hydrogen evolution reaction. *Nanoscale Horiz.* **2020**, *5*, 43–56. [CrossRef]
151. Jiang, C.; Moniz, S.J.; Wang, A.; Zhang, T.; Tang, J. Photoelectrochemical devices for solar water splitting-materials and challenges. *Chem. Soc. Rev.* **2017**, *46*, 4645–4660. [CrossRef]

152. Shu, J.; Tang, D. Recent advances in photoelectrochemical sensing: From engineered photoactive materials to sensing devices and detection modes. *Anal. Chem.* **2019**, *92*, 363–377. [CrossRef]
153. Kwasi-Effah, C.C.; Obanor, A.I.; Aisien, F.A. A review on electrolytic method of hydrogen production from water. *J. Renew. Sustain. Energy* **2015**, *1*, 51–57.
154. Zeng, Q.; Li, J.; Li, L.; Bai, J.; Xia, L.; Zhou, B. Synthesis of WO_3/$BiVO_4$ photoanode using a reaction of bismuth nitrate with peroxovanadate on WO_3 film for efficient photoelectrocatalytic water splitting and organic pollutant degradation. *Appl. Catal. B* **2017**, *217*, 21–29. [CrossRef]
155. Vinoth, S.; Ong, W.J.; Pandikumar, A. Sulfur-doped graphitic carbon nitride incorporated bismuth oxychloride/Cobalt based type-II heterojunction as a highly stable material for photoelectrochemical water splitting. *J. Colloid Interface Sci.* **2021**, *591*, 85–95. [CrossRef] [PubMed]
156. Chen, X.; Shi, R.; Chen, Q.; Zhang, Z.; Jiang, W.; Zhu, Y.; Zhang, T. Three-dimensional porous g-C_3N_4 for highly efficient photocatalytic overall water splitting. *Nano Energy* **2019**, *59*, 644–650. [CrossRef]
157. Wang, S.; Chen, P.; Bai, Y.; Yun, J.H.; Liu, G.; Wang, L. New $BiVO_4$ dual photoanodes with enriched oxygen vacancies for efficient solar-driven water splitting. *Adv. Mater.* **2018**, *30*, 1800486. [CrossRef] [PubMed]
158. Pilli, S.K.; Janarthanan, R.; Deutsch, T.G.; Furtak, T.E.; Brown, L.D.; Turner, J.A.; Hering, A.M. Efficient photoelectrochemical water oxidation over cobalt-phosphate (Co-Pi) catalyst modified $BiVO_4$/1D-WO_3 heterojunction electrodes. *Phys. Chem. Chem. Phys.* **2013**, *15*, 14723–14728. [CrossRef] [PubMed]
159. Exner, K.S.; Over, H. Kinetics of electrocatalytic reactions from first-principles: A critical comparison with the ab initio thermodynamics approach. *Acc. Chem. Res.* **2017**, *50*, 1240–1247. [CrossRef]
160. Sapountzi, F.M.; Gracia, J.M.; Fredriksson, H.O.; Niemantsverdriet, J.H. Electrocatalysts for the generation of hydrogen, oxygen and synthesis gas. *Prog. Energy Combust. Sci.* **2017**, *58*, 1–35. [CrossRef]
161. Wang, S.; Lu, A.; Zhong, C.J. Hydrogen production from water electrolysis: Role of catalysts. *Nano Converg.* **2021**, *8*, 1–23. [CrossRef]
162. Kou, Z.; Wang, T.; Gu, Q.; Xiong, M.; Zheng, L.; Li, X.; Pan, Z.; Chen, H.; Verpoort, F.; Cheetham, A.K.; et al. Rational design of holey 2D nonlayered transition metal carbide/nitride heterostructure nanosheets for highly efficient water oxidation. *Adv. Energy Mater.* **2019**, *9*, 1803768. [CrossRef]
163. Zheng, Y.; Jiao, Y.; Vasileff, A.; Qiao, S.Z. The hydrogen evolution reaction in alkaline solution: From theory, single crystal models, to practical electrocatalysts. *Angew. Chem. Int. Ed.* **2018**, *57*, 7568–7579. [CrossRef]
164. Yang, J.; Wang, C.; Ju, H.; Sun, Y.; Xing, S.; Zhu, J.; Yang, Q. Integrated quasi-plane hetero nanostructures of $MoSe_2$/Bi_2Se_3 hexagonal nanosheets: Synergetic electrocatalytic water splitting and enhanced supercapacitor performance. *Adv. Funct. Mater.* **2017**, *27*, 1703864. [CrossRef]
165. Saini, S.K.; Tailor, N.K.; Sharma, P.; Tyagi, L.; Vashistha, N.; Yadav, R.; Chaudhary, A.K.; Satapathi, S.; Kumar, M. Revealing the Substrate Dependent Ultrafast Phonon Dynamics in Bi_2Se_3 Thin Films. *Adv. Mater. Interfaces* **2022**, 2201650. [CrossRef]
166. Khatun, S.; Roy, P. Bismuth iron molybdenum oxide solid solution: A novel and durable electrocatalyst for overall water splitting. *ChemComm.* **2020**, *56*, 7293–7296. [CrossRef] [PubMed]
167. Yang, Y.; Liu, L.; Wu, J.; Qian, X. Hierarchical Bi_2S_3@ CoS_2/MoS_2 core-shelled microspheres as bifunctional electrode catalysts for efficient triiodide reduction and alkaline hydrogen evolution reactions. *J. Alloys Compd.* **2022**, *924*, 166548. [CrossRef]
168. Razzaque, S.; Khan, M.D.; Aamir, M.; Sohail, M.; Bhoyate, S.; Gupta, R.K.; Sher, M.; Akhtar, J.; Revaprasadu, N. Selective synthesis of bismuth or bismuth selenide nanosheets from a metal organic precursor: Investigation of their catalytic performance for water splitting. *Inorg. Chem.* **2021**, *60*, 1449–1461. [CrossRef] [PubMed]
169. Li, D.; Lao, J.; Jiang, C.; Luo, C.; Qi, R.; Lin, H.; Huang, R.; Waterhouse, G.I.; Peng, H. Plasmonic Au nanoparticle-decorated Bi_2Se_3 nanoflowers with outstanding electrocatalytic performance for hydrogen evolution. *Int. J. Hydrogen Energy* **2019**, *44*, 30876–30884. [CrossRef]
170. Li, J.; Wang, B.; Wang, T.; Zhao, Y.; Song, T.; Zhang, L.; Cheng, X. Construction of scaffold-like Au@MoS_2/Bi_2S_3 networks with superior electro-catalytic performance. *J. Alloys Compd.* **2020**, *831*, 154829. [CrossRef]
171. Dileep, N.P.; Puthenveettil, L.K.; Myakala, S.N.; Shaijumon, M.M. Electrophoretically-deposited BiSbSe3 nanoparticles as highly efficient electrocatalysts for hydrogen evolution reaction. *Appl. Mater. Today* **2022**, *27*, 101502. [CrossRef]
172. Naaz, F.; Sharma, A.; Shahazad, M.; Ahmad, T. Hydrothermally Derived Hierarchical CuO Nanoflowers as an Efficient Photocatalyst and Electrocatalyst for Hydrogen Evolution. *ChemistrySelect* **2022**, *7*, e202201800. [CrossRef]
173. Jain, S.K.; Pandit, N.A.; Fazil, M.; Ali, S.A.; Ahmed, J.; Alshehri, S.M.; Mao, Y.; Ahmad, T. Chemical Fabrication, Structural Characterization and Photocatalytic Water Splitting Application of Sr-Doped SnO_2 Nanoparticles. *Nanotechnology* **2022**, *33*, 355706. [CrossRef] [PubMed]
174. Farooq, U.; Ahmed, J.; Alshehri, S.M.; Mao, Y.; Ahmad, T. Self-Assembled Interwoven Nanohierarchitectures of $NaNbO_3$ and NaNb1–xTaxO_3 ($0.05 \leq x \leq 0.20$): Synthesis, Structural Characterization, Photocatalytic Applications, and Dielectric Properties. *ACS Omega* **2022**, *7*, 16952–16957. [CrossRef]
175. Mehtab, A.; Banerjee, S.; Mao, Y.; Ahmad, T. Type-II $CuFe_2O_4$/Graphitic-Carbon Nitride heterojunctions for high efficiency photocatalytic and electrocatalytic hydrogen generation. *ACS Appl. Mater. Interfaces* **2022**, *14*, 44317–44329. [CrossRef] [PubMed]

176. Ahmed, J.; Ahamad, T.; Alhokbany, N.; Almaswari, B.M.; Ahmad, T.; Hussain, A.; Al-Farraj, E.S.S.; Alshehri, S.M. Molten salts derived copper tungstate nanoparticles as bifunctional electro-catalysts for electrolysis of water and supercapacitor applications. *ChemElectroChem* **2018**, *5*, 3938–3945. [CrossRef]
177. Mehtab, A.; Ahmed, J.; Alshehri, S.M.; Mao, Y.; Ahmad, T. Rare earth doped metal oxide nanoparticles for photocatalysis: A perspective. *Nanotechnology* **2022**, *33*, 142001. [CrossRef]
178. Farooq, U.; Ahmad, T.; Naaz, F.; ul Islam, S. Review on Metals and Metal Oxides in Sustainable Energy Production: Progress and Perspectives. *Energy Fuels* **2023**. [CrossRef]

Disclaimer/Publisher's Note: The statements, opinions and data contained in all publications are solely those of the individual author(s) and contributor(s) and not of MDPI and/or the editor(s). MDPI and/or the editor(s) disclaim responsibility for any injury to people or property resulting from any ideas, methods, instructions or products referred to in the content.